PLCγ1/PKCθ Downstream Signaling Controls Cutaneous T-Cell Lymphoma Development and Progression

JID Open

Nuria García-Díaz[1], Berta Casar[2], Ruth Alonso-Alonso[3], Laura Quevedo[2], Marta Rodríguez[3], Fulgencio Ruso-Julve[1], Anna Esteve-Codina[4,5], Marta Gut[4,5], Alejandro A. Gru[6,7], María Carmen González-Vela[8], Ivo Gut[4,5], José Luis Rodriguez-Peralto[9], Ignacio Varela[2], Pablo Luis Ortiz-Romero[10], Miguel A. Piris[3] and José Pedro Vaqué[1]

Developing mechanistic rationales can improve the clinical management of cutaneous T-cell lymphomas. There is considerable genetic and biological evidence of a malignant network of signaling mechanisms, highly influenced by deregulated TCR/PLCγ1 activity, controlling the biology of these lesions. In addition, activated signal transducer and activator of transcription 3 is associated with clinical progression, although the alterations responsible for this have not been fully elucidated. Here, we studied PLCγ1-dependent mechanisms that can mediate STAT3 activation and control tumor growth and progression. Downstream of PLCγ1, the pharmacological inhibition and genetic knockdown of protein kinase C theta (PKCθ) inhibited signal transducer and activator of transcription 3 activation, impaired proliferation, and promoted apoptosis in cutaneous T-cell lymphoma cells. A PKCθ-dependent transcriptome in mycosis fungoides/Sézary syndrome cells revealed potential effector genes controlling cytokine signaling, TP53, and actin cytoskeleton dynamics. Consistently, an in vivo chicken embryo model xenografted with mycosis fungoides cells showed that PKCθ blockage abrogates tumor growth and spread to distant organs. Finally, the expression of a number of PKCθ target genes found in mycosis fungoides cells significantly correlated with that of *PRKCQ* (PKCθ) in 81 human mycosis fungoides samples. In summary, PKCθ can play a central role in the activation of malignant cutaneous T-cell lymphoma mechanisms via multiple routes, including, but not restricted to, STAT3. These mechanisms may, in turn, serve as targets for specific therapies.

Journal of Investigative Dermatology (2022) **142,** 1391–1400; doi:10.1016/j.jid.2021.09.024

INTRODUCTION

Cutaneous T-cell lymphomas (CTCLs) are a heterogeneous group of extranodal non-Hodgkin lymphomas characterized by the clonal expansion of malignant T cells in the skin (Willemze et al., 2005). Mycosis fungoides (MF) and Sézary syndrome (SS) account for the vast majority of CTCLs. Clinically, classic MF presents with patches and plaques and may eventually attain a tumoral stage. Some patients progress, their disease involving peripheral blood, lymph nodes, and viscera. SS is an aggressive leukemic subtype characterized by erythroderma, lymphadenopathy, and the presence of clonal cerebriform T cells (Sézary cells) in the skin, lymph nodes, and peripheral blood. Whereas the prognosis of patients with MF depends on stage, particularly the type and extent of skin lesions, in patients with SS it is generally poor, with a median survival of 3 years (Agar et al., 2010). Several skin-directed and systemic therapies are being explored with the aim of improving the clinical management of these malignancies, especially at advanced stages (Oka and Miyagaki, 2019), but a deeper understanding of the main mechanisms controlling the biology of these lesions would boost our ability to diagnose and treat CTCL.

In the last few years, we have learned that multiple genetic alterations affecting TP53, TCR/PLCγ1 (PLCG1 hereafter), NOTCH, NF-κB, and JAK/signal transducer and activator of transcription (STAT) activities may drive the development and progression of CTCL (Choi et al., 2015; da Silva Almeida et al., 2015; Kiel et al., 2015; Mcgirt et al., 2015; Park et al., 2017; Pérez et al., 2015; Prasad et al., 2016; Ungewickell et al., 2015; Vaqué et al., 2014; Wang et al., 2015; Woollard et al., 2016). Although still not

[1]*Molecular Biology Department, Universidad de Cantabria-Instituto de Investigación Marqués de Valdecilla, IDIVAL, Santander, Spain;* [2]*Instituto de Biomedicina y Biotecnología de Cantabria, Universidad de Cantabria-CSIC, Santander, Spain;* [3]*Pathology Department, Fundación Jiménez Díaz, CIBERONC, Madrid, Spain;* [4]*CNAG-CRG, Centre for Genomic Regulation (CRG), Barcelona Institute of Science and Technology (BIST), Barcelona, Spain;* [5]*Universitat Pompeu Fabra (UPF), Barcelona, Spain;* [6]*Department of Pathology, School of Medicine, University of Virginia, Charlottesville, Virginia, USA;* [7]*Department of Dermatology, School of Medicine, University of Virginia, Charlottesville, Virginia, USA;* [8]*Division of Pathology, Hospital Universitario Marqués de Valdecilla, Santander, Spain;* [9]*Department of Pathology, Hospital 12 de Octubre, institute i+12, CIBERONC, Medical School, University Complutense, Madrid, Spain; and* [10]*Department of Dermatology, Hospital 12 de Octubre, institute i+12, CIBERONC, Medical School, University Complutense, Madrid, Spain*

Correspondence: José Pedro Vaqué, Avda. Marqués de Valdecilla s/n, Facultad de medicina-Universidad de Cantabria and IDIVAL-Institute, 39011, Santander, Spain. E-mail: vaquej@unican.es

Abbreviations: CAM, chorioallantoic membrane; CaN, calcineurin; CTCL, cutaneous T-cell lymphoma; MF, mycosis fungoides; NTC, nontargeting control; PKC, protein kinase C; shPRKCQ, short hairpin PRKCQ; SS, Sézary syndrome; STAT, signal transducer and activator of transcription; TPA, 12-O-tetradecanoylphorbol-13-acetate

Received 18 March 2021; revised 7 September 2021; accepted 8 September 2021; accepted manuscript published online 21 October 2021; corrected proof published online 10 December 2021

fully understood, malignant TCR/PLCG1 activity constitutes an important CTCL mechanism. PLCG1 is a phospholipase that, on T-cell activation, cleaves phosphatidylinositol 4,5-bisphosphate in the plasma membrane into inositol 1,4,5-trisphosphate and diacylglycerol. Whereas inositol 1,4,5-trisphosphate triggers calcium release from the endoplasmic reticulum, leading to NFAT activation via calcineurin (CaN), diacylglycerol can activate specific protein kinase C (PKC) isoforms (Isakov and Altman, 2002). Constitutively activated PLCG1 SNVs (S345F and others), present in 10–20% of cases, promote the activation of important T-cell nuclear effectors, such as NFAT (Park et al., 2017; Patel et al., 2020; Vaqué et al., 2014) and NF-κB (Patel et al., 2020). In addition, deregulated expression and amplification of the *PRKCQ* gene (protein PKCθ) have been described in 30% of cases (Choi et al., 2015; Wang et al., 2015; Woollard et al., 2016). PKCθ is a serine/threonine kinase widely expressed in T lymphocytes (Meller et al., 1998) and a well-known PLCG1 effector (Steinberg, 2008). In contrast, members of the JAK/STAT signaling pathway frequently harbor genetic alterations, such as activating mutations (4%) and amplifications (up to 60%) in CTCL cases (Park et al., 2017). JAKs are tyrosine kinases that phosphorylate and activate STAT transcriptional activity in response to extracellular stimuli (Vainchenker and Constantinescu, 2013). Serine phosphorylation can modulate STAT activities in response to alternative stimuli (Decker and Kovarik, 2000). Whereas PLCG1 mutations and nuclear NFAT and NF-κB accumulation have been found in MF cases at all stages, activated STAT3 has recently been associated with MF in advanced stages (Pérez et al., 2020) and has been detected in SS cells (Eriksen et al., 2001).

Thus, acting downstream of PLCG1, we investigated the role of PKCθ mediating STAT3 activation and studied the mechanisms associated to its potential role at controlling the development and progression of MF lesions.

RESULTS

PLCγ1/PKCθ downstream signaling promotes STAT3 activation and proliferation/survival of CTCL cells

Recent evidence suggests that TCR downstream signaling plays an important role in the biology of CTCL via PLCG1. Because activated STAT3 has been associated with advanced CTCL stages, we decided to study the potential mechanisms underlying PLCG1 and its downstream effector PKCθ in the activation of STAT3. To this end, we set up a combination of wild type and constitutively activated PLCG1 (PLCG1 S345F) and PKCθ (PRKCQ A148E; details in Supplementary Materials and Methods and Supplementary Table S1) mutants, transiently expressed alongside specific luciferase-based reporter genes for STAT3 and NFAT in HEK293 cells. We combined this approach with the use of specific inhibitors employed in clinic practice: tacrolimus (a CaN inhibitor), sotrastaurin (a pan-PKC inhibitor mostly for PKCθ), and ruxolitinib (a JAK inhibitor), as depicted in Supplementary Figure S1a.

In these settings, PLCG1 and PRKCQ mutants triggered STAT3 transcriptional activation, which was dependent on PKCθ and JAK activities (Figure 1a). Their combined inhibition did not induce a significant STAT3 blockage as compared with each inhibitor used alone. Activated PLCG1 and PRKCQ promoted STAT3 phosphorylation in residues Y705 (a JAK-dependent phosphorylation site) and S727 (JAK independent), which were impaired by sotrastaurin (Figure 1b and Supplementary Figure S1b and c). In contrast, as controls, PLCG1 and PRKCQ mutants elicited NFAT transcriptional activation that was impaired by tacrolimus and sotrastaurin (Supplementary Figure S1d).

To further explore the mechanisms that, downstream of PKCθ, can mediate STAT3 activation and malignant proliferation, we took advantage of HEK293, Jurkat, and CTCL (MyLa [MF-derived] and HuT 78 [SS-derived]) cells, which express PKCθ mRNA and protein at detectable levels (Supplementary Figure S2a). Generally, 12-*O*-tetradecanoylphorbol-13-acetate (TPA) promoted phosphorylation of STAT3 in tyrosine (Y705) and serine (S727) residues. In CTCL cells, whereas MyLa cells displayed a constitutive phosphorylation in Y705, TPA increased S727 both in MyLa and HuT 78 and Y705 in Hut 78 cells. (Figure 1c and Supplementary Figure S2b). Whereas sotrastaurin (PKCθ inhibitor) impaired phosphorylation in tyrosine and serine residues, ruxolitinib (JAK inhibitor) only abrogated tyrosine phosphorylation. Finally, both inhibitors abrogated the binding of activated STAT3 proteins to a specific STAT3 DNA-binding sequence in HuT 78 cells (Figure 1d).

Biologically, pharmacological inhibition of PKCθ provoked a concentration-dependent reduction of CTCL cell proliferation and triggered apoptosis (Supplementary Figure S2c and d). Notably, and consistent with our previous results, the combined inhibition of PKCθ and JAK had a synergistic antiproliferative effect in CTCL cells (Figure 1e).

PKCθ-dependent transcriptome in MF/SS cells uncovers CTCL disease mechanisms

To further study the role of PKCθ in CTCL cells, we generated stable MyLa, HuT 78, and HEK293 cells with doxycycline-inducible expression of *PRKCQ* short hairpin RNA (shPRKCQ) and a nontargeting control (NTC). On incubation with doxycycline, PKCθ protein levels were effectively knocked down in all cells (Figure 2a and Supplementary Figure S2e). PKCθ knocked down cells showed reduced phosphorylation of STAT3 in Y705 and S727 residues, as well as decreased STAT3 transcriptional activity in HEK293 cells stably transfected with a STAT3 reporter (STAT3-SEAP) (Figure 2a and b and Supplementary Figure S2e and f). PKCθ deficiency also impaired MyLa and HuT 78 cell proliferation (Figure 2c).

We next searched for specific PKCθ target genes and pathways that, alongside STAT3 activation, could enlighten its role in CTCL. To this end, we performed mRNA sequencing in vehicle or TPA-stimulated NTC and shPRKCQ MyLa and HuT 78 cells. In our analysis, we identified 23 significant PKCθ-regulated genes shared between both cell lines: 13 in vehicle (DMSO) and 10 in TPA-treated cells (Figure 2d). Under both conditions, PKCθ positively controlled the expression of *LDLRAD3* (lipoprotein receptor), *RBM47* (RNA binding/TP53-related), and *EAF1* (transcriptional coactivator) and negatively regulated *RNF38* (ubiquitin ligase/TP53-related). In addition, PKCθ positively controlled

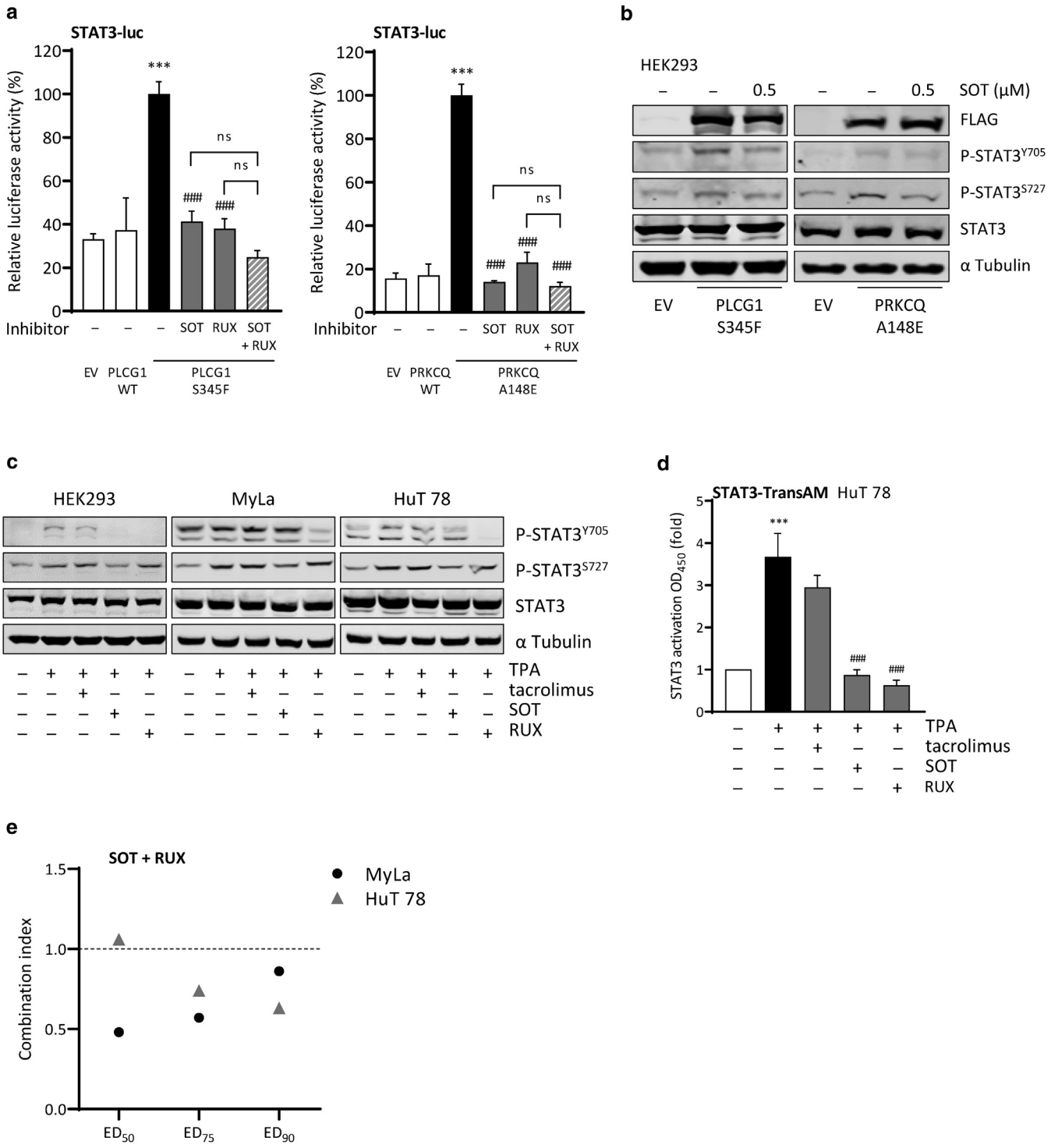

Figure 1. PLCG1/PKCθ downstream signaling triggers STAT3 activation. (**a**) STAT3 luciferase reporter activity in HEK293 cells transfected with the indicated vectors and treated with PKCθ and JAK inhibitors (SOT and RUX, respectively, 1 μM, 24 hours) or the combination of both (n = 3). (**b**) Western blot of HEK293 cells transfected with the indicated vectors, starved, and treated with SOT (0.5 μM, 3 hours) and incubated with the indicated antibodies. (**c**) Western blot of starved HEK293, MyLa, and HuT 78 cells treated with the indicated inhibitors (1 μM, 3 hours), stimulated with TPA (10 ng/ml, 1 hour), and incubated with the indicated antibodies. (**d**) ELISA-based assay showing activated STAT3 bound to specific DNA-binding sequence in HuT 78 cells treated with the indicated inhibitors (1 μM, 3 hours) and TPA (10 ng/ml, overnight) (n = 3). (**e**) CIs at 50%, 75%, and 90% ED in MyLa and HuT 78 cells treated with a combination of SOT and RUX (24 hours). CIs were calculated using the Chou-Talalay method. CI < 1 indicates synergism, CI = 1 is additive, and CI > 1 indicates antagonism. Images are representative of each western blot (n = 3). Data are mean ± SEM. Student's *t*-test: ***$P < 0.001$ versus PLCG1/PRKCQ WT (**a**) or control vehicle (**d**), ##$P < 0.01$ and ###$P < 0.001$ versus PLCG1 S345F or PRKCQ A148E treated with control vehicle (**a**) or TPA (**d**). CI, combination index; ED, effective dose; EV, empty vector; ns, not significant; PKC, protein kinase C; P-STAT, phosphorylated signal transducer and activator of transcription; RUX, ruxolitinib; SOT, sotrastaurin; STAT, signal transducer and activator of transcription; TPA, 12-*O*-tetradecanoylphorbol-13-acetate; WT, wild type.

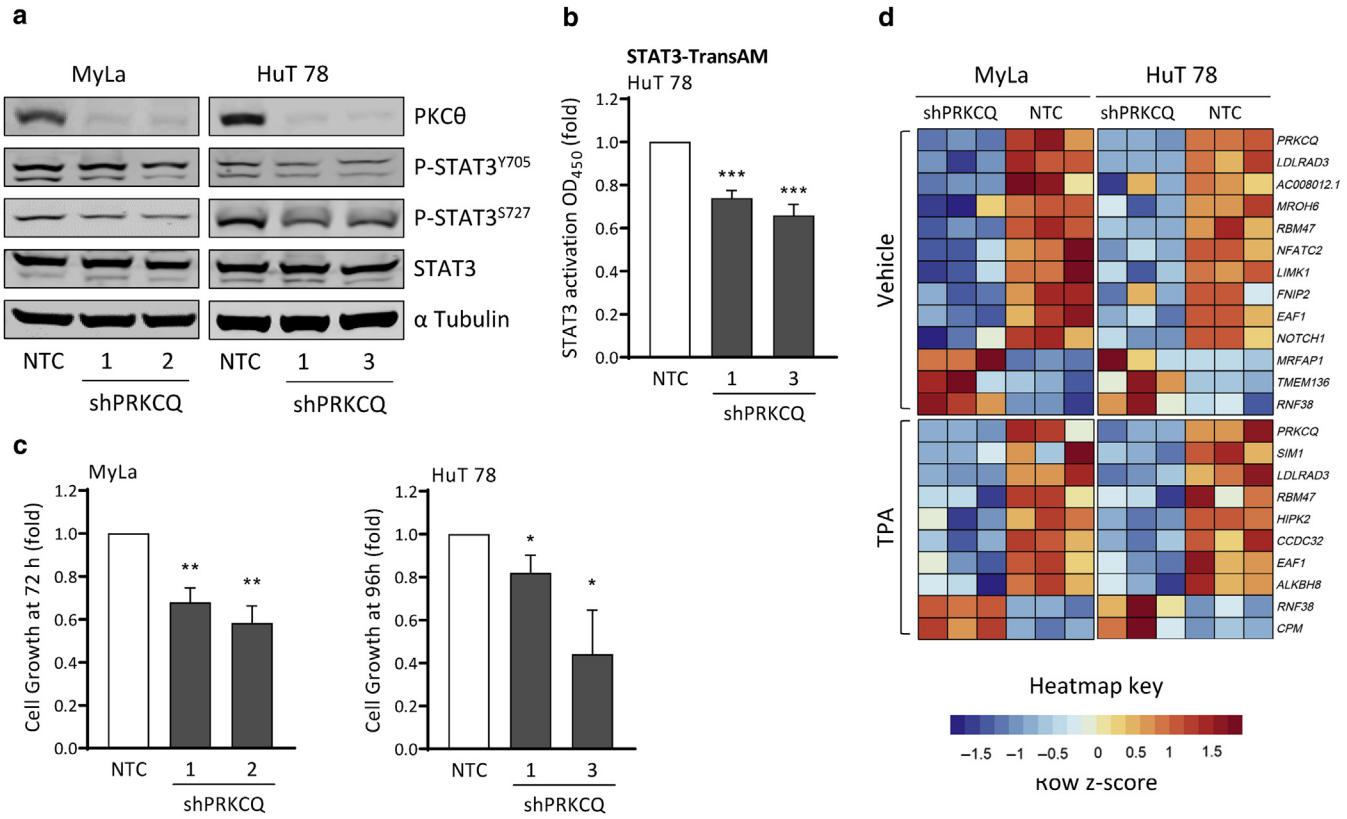

Figure 2. PKCθ-dependent transcriptome in MF/SS cells. (**a**) Western blot of cells with inducible expression of NTC or shPRKCQ and incubated with the indicated antibodies. Lanes numbered 1, 2, and 3 refer to different shPRKCQ sequences. Images are representative of each western blot (n = 3). (**b**) ELISA-based assay showing activated STAT3 bound to specific DNA-binding sequence in NTC and shPRKCQ HuT 78 cells (n = 4). (**c**) Proliferation of NTC and shPRKCQ MyLa and HuT 78 cells after *PRKCQ* knockdown induction (n = 4). (**d**) Heatmap representation of a selection of differentially expressed genes in shPRKCQ MyLa and HuT 78 cells compared with NTC cells treated with control vehicle or TPA (10 ng/ml, n = 3). Expression differences range from blue (downregulation) to red (upregulation) according to the z-score. Data are mean ± SEM. Student's *t*-test: $*P < 0.05$, $**P < 0.01$, and $***P < 0.001$ versus NTC. h, hour; MF, mycosis fungoides; NTC, nontargeting control; P-STAT, phosphorylated signal transducer and activator of transcription; PKC, protein kinase C; shPRKCQ, short hairpin *PRKCQ;* SS, Sézary syndrome; STAT, signal transducer and activator of transcription; TPA, 12-*O*-tetradecanoylphorbol-13-acetate.

the expression of *NFATC2* (TCR/PLCG1 effector), *LIMK1* (actin cytoskeleton), and *NOTCH1* under basal conditions and *HIPK2* (kinase/TP53 related) and *ALKBH8* (methyltransferase) in response to TPA. An independent validation of the data is included in Supplementary Figure S3a.

An alternative gene set enrichment analysis was performed to interpret the gene expression data. We identified a number of significantly deregulated gene sets based on Kyoto Encyclopedia of Genes and Genomes pathways ($P < 0.05$ and false discovery rate < 0.25) in shPRKCQ versus NTC cells (Table 1). Among these, we found potential PKCθ effectors that can participate in cytokine/cytokine receptor interaction (*CCL22*), hematopoietic cell lineage (*IL6R*), DNA replication (*PCNA*), cell cycle (*PLK1*), adipocytokine signaling (*JAK2, STAT3*, and *TNF*), base excision repair (*POLD1*), and TP53 signaling (*CHEK1*) (Supplementary Table S2 and Supplementary Figure S3b).

Blockage of PKCθ impairs CTCL tumorigenesis and dissemination in vivo

To study the malignant activities carried out by PKCθ in vivo, we used a chicken embryo model, which offers the possibility of generating primary tumors and studying its spreading potential in a timely and cost-effective manner. Thus, we generated xenografted tumors derived from MyLa cells implanted on top of the chicken chorioallantoic membrane (CAM). These tumors displayed positive CD30 and phosphorylated STAT3 immunohistochemical staining (Figure 3a and Supplementary Figure S4). We blocked PKCθ using two distinct approaches: pharmacological (i.e., sotrastaurin) and genetic (i.e., short hairpin RNA). To study the effects of sotrastaurin, we seeded 1×10^6 MyLa cells into the CAM of day 10 chicken embryos and allowed them to grow for 7 days. In this setting, sotrastaurin was used once (2 days before harvesting) or twice (every 2 days after cell implantation). In parallel, 1×10^6 NTC or shPRKCQ MyLa cells, previously incubated with doxycycline, were also seeded into the CAMs of the chicken embryos and allowed to grow under the same conditions. As shown in Figure 3b, PKCθ blockage greatly impaired primary tumor growth. Moreover, because this system enables the detection of disseminating cells (human cells in this case) in chicken embryo tissue, we detected that control MyLa cells intravasated the distal CAM and disseminated to internal organs (liver and lungs, Figure 3c and d). Strikingly, PKCθ blockage provoked a substantial reduction in the spreading of MyLa cells that occurred alongside a

Table 1. GSEA of PKCθ-Dependent Transcriptome

KEGG PATHWAY	NES	NOM *P*-Val	FDR q-Val	Representative Enriched Genes
Vehicle				
ANTIGEN PROCESSING AND PRESENTATION	1.54	0.026	0.249	*HSPA1A, KIR3DL1, LGMN, KIR2DL3*
CYTOKINE-CYTOKINE RECEPTOR INTERACTION	1.73	0.000	0.097	*CCL22, IL6R, CCL3, TNFSF13B, IL11, TNFRSF9, IL13, CD40LG, PDGFA, TNFRSF11A, TNFSF9*
HEMATOPOIETIC CELL LINEAGE	1.73	0.011	0.116	*IL6R, ITGA1, CD37, ITGA6, IL11, ITGB3, CD3G*
RIBOSOME	1.87	0.000	0.114	*RPS3, RPS27A, RPS15*
TPA				
DNA REPLICATION	−2.27	0.000	0.000	*RFC1, POLE2, LIG1, PCNA, POLD3, MCM7*
CELL CYCLE	−2.19	0.000	0.000	*PLK1, PRKDC, CDC25C, SKP2, CDK2, E2F1*
MISMATCH REPAIR	−1.68	0.013	0.105	*RFC4, MSH2, LIG1, POLD3, PCNA, EXO1*
ADIPOCYTOKINE SIGNALING PATHWAY	−1.56	0.032	0.179	*TRAF2, JAK2, NFKBIB, CAMKK1, AKT3, STAT3, TNF, SOCS3, PRKCQ*
BASE EXCISION REPAIR	−1.53	0.039	0.177	*PARP1, POLD1, POLE, PCNA*
P53 SIGNALING PATHWAY	−1.46	0.038	0.245	*CHEK1, CDK1, BID, CCNE2, CDK6*
HEMATOPOIETIC CELL LINEAGE	1.63	0.013	0.249	*CD38, CD37, FLT3LG, IL11, ITGAM, CD3G, IL11RA, IL9R*
RIBOSOME	2.25	0.000	0.000	*RPS3, RPS27A, RPS15*

Abbreviations: FDR q-Val, false discovery rate q-value; GSEA, gene set enrichment analysis; KEGG, Kyoto Encyclopedia of Genes and Genomes; NES, normalized enrichment score in shPRKCQ versus NTC cells; NOM *P*-Val, nominal *P*-value; PKC, protein kinase C; TPA, 12-*O*-tetradecanoylphorbol-13-acetate.

reduction in CD30 and phosphorylated STAT3 staining (Figure 3a and Supplementary Figure S4).

A PKCθ expression signature in human MF

Given the role of PKCθ in MF tumor formation and dissemination, we next questioned whether a PKCθ-derived expression signature could be detected in a cohort of MF samples. First, 16 PKCθ target genes, previously identified by mRNA sequencing in MyLa cells, were selected based on significance and their associated biological activities (Figure 4a). This selection included genes involved in the control of the cytoskeleton (*CIT*, *LCP1*, and *LSP1*), signaling oncogenes (*FGFR1*, *FGFR3*, *MAPK13*, or *PRKACB*), cell adhesion (*VCAM*), or angiogenesis (*VEGFB*). Then, using NanoString, we comparatively studied their expression profiles in a cohort of 81 individual samples (including plaques and tumors) from 27 patients with MF and six inflammatory dermatoses used as control (Supplementary Table S3). Analysis of the results showed that *PRKCQ* and its target genes, with the exception of *RHOB*, were differentially and significantly expressed in MF as compared with inflammatory dermatoses (Supplementary Figure S5).

The heatmap showing the general expression pattern of PKCθ and its target genes in MF cases is shown in Figure 4b. The expression of eight genes significantly correlated with that of *PRKCQ* across the cohort. Whereas *PRKACB*, *LCP1*, *CCDC32*, *LSP1*, and *TNFRSF25* showed a positive correlation, others such as *MAPK13*, *FGFR3*, and *RHOB* displayed a negative correlation (Figure 4c).

DISCUSSION

Clinical management of CTCL requires efficient therapies, especially in advanced stages. Deregulated TCR/PLCG1 downstream signaling constitutes a major alteration, as assessed by the presence of constitutively activated PLCG1 mutants with nuclear NFAT activation (10% of the cases) (Choi et al., 2015; Mcgirt et al., 2015; Ungewickell et al., 2015; Vaqué et al., 2014; Woollard et al., 2016) and amplifications in the *PRKCQ* gene (PKCθ), in 20−30% of the cases (Choi et al., 2015; Woollard et al., 2016) nonoverlapping with PLCG1 SNVs. Because PLCG1 is still a nondruggable target in the clinic, specific targeting of CaN has the potential to block NFAT activation downstream of TCR/PLCG1 (Vaqué et al., 2014). Based on our previous findings, our team is about to report promising results of a clinical trial using topical pimecrolimus (a CaN inhibitor) in patients with early-stage MF (PimTo-MF study, EudraCT number: 2014-001377-14; Ortiz-Romero et al., unpublished data). Lessons learned from this experience and the various lines of genetic evidence reported in the literature indicate that downstream of TCR/PLCG1, alternative pathways can participate in parallel with CaN/NFAT, acting as mechanisms of resistance to therapy and/or disease progression. In our study, PLCG1-S345F activated NFAT by a mechanism involving CaN and PKCθ. Additionally, a mutant PKCθ with constitutive activated kinase activity (A148E) activated NFAT, which was abrogated by sotrastaurin. These preclinical data suggest that combinations of CaN and PKCθ inhibitors may increase therapy efficacy during early stages and/or provide a rationale for treating nonresponders or even patients with advanced CTCL.

Despite the fact that genetic alterations in the JAK/STAT pathway are frequent in CTCL, the percentage of cases with mutant JAK and STAT proteins (about 8%) cannot fully explain the high proportion of lesions with activated/phosphorylated STAT expression in the nucleus of malignant T cells (Fantin et al., 2008; Pérez et al., 2020; Sommer et al., 2004). Therefore, alternative mechanisms are under discussion and include proinflammatory microenvironments (Kim et al., 2005) or immune responses to bacterial colonization in the compromised skin barriers of CTCL lesions (Fanok et al., 2018; Willerslev-Olsen et al., 2016). It is also

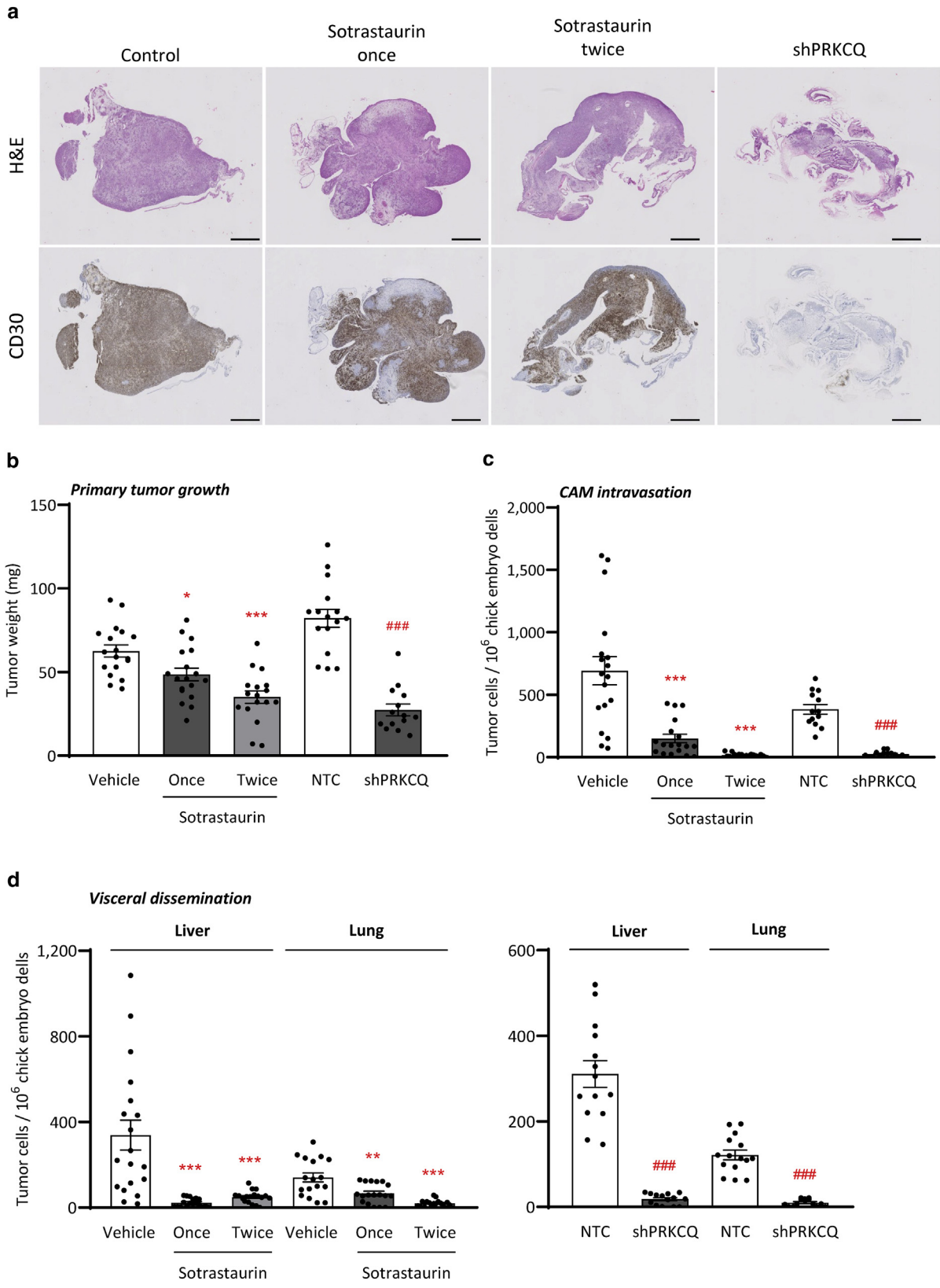

Figure 3. Blockage of PKCθ impairs CTCL tumorigenesis and dissemination in vivo. (**a**) H&E and CD30 staining of paraffin sections of control, tumors treated once or twice with sotrastaurin, and tumors with PKCθ deficiency (shPRKCQ). (**b**–**d**) Pharmacological and genetic PKCθ inhibition effects on (**b**) tumor weight, (**c**) CAM intravasation, and (**d**) visceral dissemination to liver and lungs of chicken embryos engrafted with MyLa cells treated once or twice with sotrastaurin (10 μM, n = 17–18) or engrafted with NTC or shPRKCQ MyLa cells (n = 14–16). Data are mean ± SEM. Student's *t*-test: $^{*}P < 0.05$, $^{**}P < 0.01$, and $^{***}P < 0.001$ versus control vehicle; $^{\#\#\#}P < 0.001$ versus NTC. Bar = 1 mm. CAM, chorioallantoic membrane; CTCL, cutaneous T-cell lymphoma; NTC, nontargeting control; PKC, protein kinase C; shPRKCQ, short hairpin *PRKCQ*.

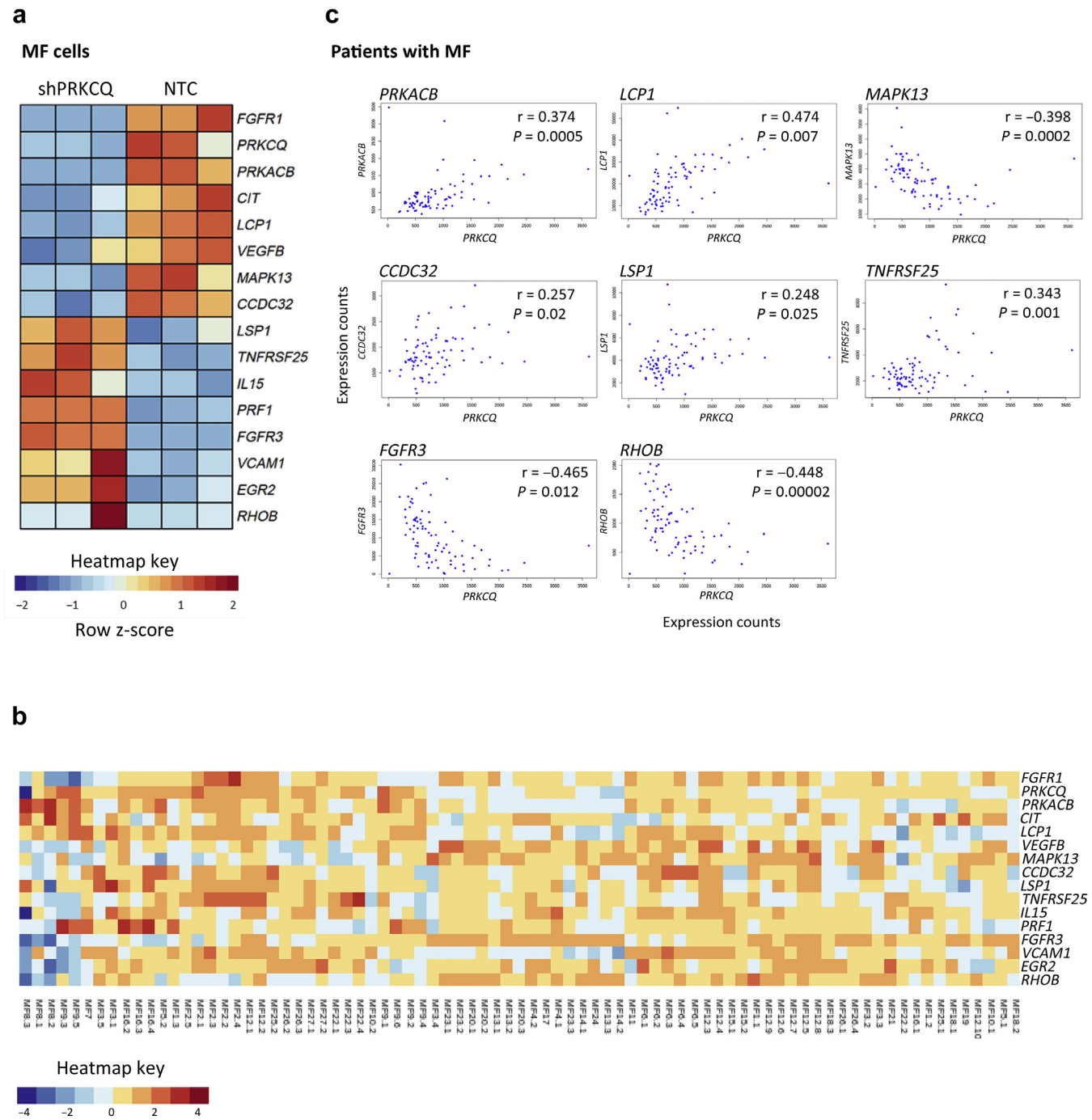

Figure 4. Correlation between the expression of PKCθ and its target genes in MF cells and human samples. (**a**) Heatmap representation of a selection of differentially expressed genes in shPRKCQ MyLa cells compared with NTC and treated with TPA (10 ng/ml, 24 hours, n = 3). Expression differences range from blue (downregulation) to red (upregulation) according to the z-score. (**b**) Heatmap representation of the expression of the indicated genes in MF samples. (**c**) Correlation of gene expressions between *PRKCQ* and *PRKACB*, *LCP1*, *MAPK13*, *CCDC32*, *LSP1*, *TNFRSF25*, *FGFR3*, and *RHOB* in MF samples. MF, mycosis fungoides; NTC, nontargeting control; PKC, protein kinase C; shPRKCQ, short hairpin *PRKCQ*; TPA, 12-*O*-tetradecanoylphorbol-13-acetate.

possible that, downstream of PLCG1, deregulated intracellular mechanisms may also trigger STAT activation. In support of this hypothesis, a combination of targeted sequencing and immunohistochemical staining in a cohort of patients with early and advanced MF detected two PLCG1-S345F–positive patients displaying nuclear phosphorylated STAT3 staining in the absence of mutated JAKs (Pérez et al., 2020). In our work, PLCG1 and PKCθ mutants promoted the phosphorylation and transcriptional activity of STAT3 by JAK-dependent and JAK-independent mechanisms. The combination of PKCθ and JAK inhibitors was not significantly superior to each inhibitor used alone at blocking STAT3, suggesting that these can participate as part of the same signaling axis. Moreover, genetic PKCθ knockdown also abrogated STAT3 phosphorylation, transcriptional activity, and proliferation in CTCL cells. Following this line of evidence, TPA (a PKC activator) also promoted STAT3 phosphorylation in tyrosine and serine residues alongside STAT3 transcriptional activity in CTCL cells.

Finally, this conjoined PKCθ and JAK mechanism also proved to be biologically relevant, because their combined inhibition provoked the synergistic abrogation of cell proliferation. Thus, malignant STAT3 activation in advanced CTCL can be triggered by deregulated extracellular stimuli (usually JAK-dependent), mutations in JAKs, and/or alternative mechanisms, such as deregulated PLCG1/PKCθ downstream signaling.

This PLCG1/PKCθ—STAT3 connection may have important implications for setting up approaches for treating CTCL, with a special focus on advanced cases. On the one hand, specific JAK inhibitors are being used in the clinical milieu (de Freitas and da Costa Maranduba, 2015; Lee et al., 2014; Malemud, 2018). Therefore, it is conceivable that they may be effective for treating patients with CTCL with deregulated JAK/STAT activity. In this regard, active clinical trials test JAK inhibitors in relapsed T- or NK-cell lymphomas (NCT02974647) and peripheral T-cell lymphoma (NCT04105010), offering the possibility of enrolling patients with CTCL. In contrast, it would be highly beneficial to design future therapies bearing in mind that a variety of mechanisms, such as CaN, PKCθ, or JAKs, may synergistically drive CTCL progression.

Despite the fact that individual PKCθ or JAK inhibitors provoked a total blockage of STAT3 activation, their combination still elicited a synergistic antiproliferative effect in CTCL cells. To gain further evidence about the malignant CTCL mechanisms controlled by PKCθ, other than STAT3, we searched for specific target genes and pathways shared between MF and SS cells. This analysis revealed a number of candidate PKCθ target genes with potentially relevant malignant activities in CTCL, such as the following: (i) Regulation of *TP53*, the most frequently altered gene in these entities (Chang et al., 2018; da Silva Almeida et al., 2015); *RBM47*, a positive regulator of the TP53/p21 axis that is also associated with lung carcinogenesis (Radine et al., 2020; Sakurai et al., 2016); *HIPK2*, a proapoptotic kinase that regulates and phosphorylates TP53 (Cecchinelli et al., 2006); and *RNF38*, coding a TP53 ubiquitine ligase (Sheren and Kassenbrock, 2013); (ii) Rho/actin cytoskeleton remodeling: *LIMK1*, which controls actin cytoskeleton dynamics and cell shape/movement via cofilin (Hamill et al., 2016); (iii) TCR-PLCG1 downstream signaling: *NFATC2* (NFAT1), acting downstream of CaN, can control cytokine expression such as IL-2 or IL-4 in T cells (Mognol et al., 2016); and (iv) *NOTCH1*, a CTCL oncogene related to cell survival (Kamstrup et al., 2010). Our results argue in favor of PKCθ acting as part of an intricate TCR/PLCG1 network of signaling mechanisms to play a key mechanistic and biological role, via multiple oncogenic effectors, to control CTCL cell proliferation, survival, and dissemination. Functionally, we carried out an alternative gene set enrichment analysis. This analysis highlighted important biological activities controlled by PKCθ, such as cytokine/cytokine receptor interaction, hematopoietic cell lineage, cell cycle, and TP53 signaling.

To investigate the biological role of PKCθ in vivo, we used a chicken embryo xenograft model (Crespo and Casar, 2016; Klingenberg et al., 2014). MF cells deficient in PKCθ expression had greatly impaired the ability to grow tumors, promote angiogenesis, intravasate blood vessels, and spread to distant organs. Moreover, sotrastaurin provoked similar effects. These results are consistent with the transcriptome data and, although still in a CTCL preclinical setting, can support a mechanistic role for PKCθ in controlling multiple malignant cellular activities, such as those explained earlier, promoting tumor development and progression in patients. In this regard, we studied the expression of a specific subset of 16 PKCθ target genes, chosen among those found in MyLa cells (MF-derived) in a cohort of 81 human MF samples and six inflammatory dermatoses. First, *PRKCQ* and its target genes, except *RHOB,* were differentially expressed in MF cases versus controls, which highlights the potential oncogenic role of PKCθ and its downstream effectors in CTCL. Regarding MF cases, a heterogeneous gene expression pattern was found between patients and between samples, which aligns with the inter- and intratumoral heterogeneity recently described in CTCL cases, using transcriptomic analyses (Gaydosik et al., 2019; Iyer et al., 2019). Nevertheless, we specifically detected eight genes whose expression was significantly correlated with that of *PRKCQ* in these samples. More in detail, whereas *PRKACB* (protein kinase A, catalytic subunit beta), *TNFRSF25* (a TNF receptor), and the actin binding *LSP1* and *LCP1* correlated positively with *PRKCQ*, a negative correlation was found with *RHOB*, *FGFR3*, and *MAPK13* (p38 MAPK delta). Although further studies will help explain the functional roles of these genes in the biology of MF, in a PKCθ context, it is plausible that protein kinase A/CREB activity and dynamic regulation of the actin cytoskeleton might play essential roles in the ability of PKCθ to promote CTCL tumor formation and dissemination.

In summary, this work provides strong mechanistic and biological evidence of the role of a malignant TCR/PLCG1/PKCθ signaling network controlling the biology of CTCL. From a translational perspective, this study identifies different mechanisms for activating STAT3 downstream of TCR/PLCG1; proposes rational approaches to developing targeted therapies, including CaN, PKCθ, and JAK inhibitors used alone or in combination; and reveals a number of PKCθ target genes and pathways to be explored in a translational setting, because they may play essential roles in CTCL.

MATERIALS AND METHODS

Patient samples

A total of 87 formalin-fixed, paraffin-embedded tissue samples belonging to 27 patients with MF and six inflammatory dermatoses were used (Supplementary Table S3). The samples were collected in The Hospital 12 de Octubre, Madrid, Spain, in collaboration with the Fundación Jiménez Díaz Hospital, in Madrid, and the study was conducted in accordance with the Declaration of Helsinki. All patients gave written informed consent to be included in this study. All the processes were approved and conducted in adherence with the specific recommendations of the Comité Etico de Investigación clínica del Hospital 12 de Octubre.

Chicken embryo model for spontaneous tissue colonization

Fertilized hen eggs were obtained from Granja Gibert (Spain) and incubated at 60% humidity and 38 °C in a rotating incubator. Spontaneous metastasis and tissue colonization were performed as described elsewhere (Crespo and Casar, 2016). Briefly, on day 10 of chick development, eggs were windowed and 1×10^6 MyLa cells, resuspended in 20% Matrigel (Corning, VA) and 80% serum-free

media, and placed onto the CAM. Cells were allowed to expand for 7 days in a stationary incubator at 60% humidity and 38 °C, and two experiments were performed: (i) doxycycline-induced NTC or shPRKCQ MyLa cells and (ii) MyLa cells topically treated on the upper CAM with vehicle or sotrastaurin (10 μM) in serum-free media 2 days before harvesting (once) or every 2 days (twice). Primary tumors were excised, weighed, fixed in 4% buffered formaldehyde, washed with PBS, and embedded in paraffin. Human cells within chick embryo tissues were detected by quantitative *Alu* PCR.

The CAM does not require obtaining ethics committee approval for animal experimentation. Chick embryos are not considered as living animals until day 17 of development in most countries. The CAM is not innervated, and experiments are terminated before the development of centers in the brain associated with pain perception, making this a system not requiring animal experimentation permissions. Thus, according to European law (Directive 2010/63/EU of the European Parliament and of the Council of 22 September 2010 on the protection of animals used for scientific purposes), the CAM model system does not raise any ethical or legal concerns, thus being an attractive alternative to other animal experiments.

NanoString gene expression assay

Total RNA isolation was performed on formalin-fixed, paraffin-embedded skin samples using an RNeasy FFPE Kit (Qiagen, Hilden, Germany) according to the manufacturer's instructions. We used an nCounter Custom CodeSet Design in conjunction with the nCounter Flex Analysis System (NanoString Technologies, Seattle, WA). Gene expression values were normalized with respect to eight housekeeping genes. The data were analyzed by nSolverTM Analysis Software 4.0 (NanoString Technologies) using the nCounter Advanced Analysis (version 2.0.134). Raw data were normalized using internal negative and positive controls. Hierarchical cluster analysis was performed using R 3.6.1 (package pheatmap, https://www.R-project.org, R Foundation for Statistical Computing, Vienna, Austria).

Statistical analysis

Unless otherwise specified, all experiments were performed in independent triplicates and numerical data were summarized as mean ± SEM using GraphPad Prism6 software (San Diego, CA). Global means of pairs of groups were compared using two-tailed unpaired Student's *t*-tests, with statistical significance concluded for values of $P < 0.05$: */# < 0.05, **/## < 0.01 and ***/### < 0.001. Correlation of gene expression between *PRKCQ* and the other genes was compared with Pearson's *r* correlation test.

Data availability statement

For detailed methods and original protocols, please contact vaquej@unican.es. Raw RNA-sequencing files are available at the Gene Expression Omnibus repository under the accession number GSE157442 (https://www.ncbi.nlm.nih.gov/geo/query/acc.cgi).

ORCIDs

Nuria García-Díaz: http://orcid.org/0000-0002-0511-5590
Berta Casar: http://orcid.org/0000-0002-3058-5631
Ruth Alonso-Alonso: http://orcid.org/0000-0001-9503-7268
Laura Quevedo: http://orcid.org/0000-0001-8902-5818
Marta Rodríguez: http://orcid.org/0000-0001-8543-6767
Fulgencio Ruso-Julve: http://orcid.org/0000-0001-6500-6807
Anna Esteve-Codina: http://orcid.org/0000-0003-0361-2873
Marta Gut: http://orcid.org/0000-0002-4063-7159
Alejandro A. Gru: http://orcid.org/0000-0002-2573-8074
María Carmen González-Vela: http://orcid.org/0000-0002-1695-9203
Ivo Gut: http://orcid.org/0000-0001-7219-632X
José Luis Rodriguez-Peralto: http://orcid.org/0000-0002-6578-7153
Ignacio Varela: http://orcid.org/0000-0002-0969-506X
Pablo Luis Ortiz-Romero: http://orcid.org/0000-0003-2985-9639
Miguel A. Piris: http://orcid.org/0000-0001-5839-3634
José Pedro Vaqué: http://orcid.org/0000-0002-3913-2495

CONFLICT OF INTEREST

PLOR has served as an advisor for Takeda, Kyowa, 4SC, MIRAGEN, Helsinn, Recordati Rare Diseases, and Innate Pharma and holds a patent for PLCG1. MAP has served on the advisory board for Millenium/Takeda, Celgene, Gilead, Jansen, Nanotring, and Kyowa Kirin; received lecture fees from Millenium/Takeda and Jansen; and received research funding from Millenium/Takeda, Gilead, and Kura. All other authors state no conflicts of interest.

ACKNOWLEDGMENTS

This work has been funded by the Instituto de Salud Carlos III (ISCIII)/FEDER (PI16/00156, PI19/00204, and ASOCIACION LUCHAMOS POR LA VIDA to JPV; PI17/0957 to PLOR). NGD has been supported by a predoctoral contract from UC-IDIVAL. BC holds a RyC contract from MICINN (RYC2018-024004). AEC is funded by ISCIII/MINECO/FEDER (PT17/0009/0019).

AUTHOR CONTRIBUTIONS

Conceptualization: NGD, BC, MAP, JPV; Data Curation: NGD, BC, RAA, FRJ, JPV; Formal Analysis: MCGV, AAG, JLRP, PLOR, MAP; Investigation: NGD, RAA, LQ, MR, AEC, MG, IV, IG; Writing: NGD, BC, MAP, JPV

SUPPLEMENTARY MATERIAL

Supplementary material is linked to the online version of the paper at www.jidonline.org, and at https://doi.org/10.1016/j.jid.2021.09.024.

REFERENCES

Agar NS, Wedgeworth E, Crichton S, Mitchell TJ, Cox M, Ferreira S, et al. Survival outcomes and prognostic factors in mycosis fungoides/Sézary syndrome: validation of the revised International Society for Cutaneous Lymphomas/European Organisation for Research and Treatment of Cancer staging proposal. J Clin Oncol 2010;28:4730–9.

Cecchinelli B, Lavra L, Rinaldo C, Iacovelli S, Gurtner A, Gasbarri A, et al. Repression of the antiapoptotic molecule galectin-3 by homeodomain-interacting protein kinase 2-activated p53 is required for p53-induced apoptosis. Mol Cell Biol 2006;26:4746–57.

Chang LW, Patrone CC, Yang W, Rabionet R, Gallardo F, Espinet B, et al. An integrated data resource for genomic analysis of cutaneous T-cell lymphoma. J Invest Dermatol 2018;138:2681–3.

Choi J, Goh G, Walradt T, Hong BS, Bunick CG, Chen K, et al. Genomic landscape of cutaneous T cell lymphoma. Nat Genet 2015;47:1011–9.

Crespo P, Casar B. The chick embryo chorioallantoic membrane as an in vivo model to study metastasis. Bio Protoc 2016;6:1–11.

da Silva Almeida AC, Abate F, Khiabanian H, Martinez-Escala E, Guitart J, Tensen CP, et al. The mutational landscape of cutaneous T cell lymphoma and Sézary syndrome. Nat Genet 2015;47:1465–70.

de Freitas RM, da Costa Maranduba CM. Myeloproliferative neoplasms and the JAK/STAT signaling pathway: an overview. Rev Bras Hematol Hemoter 2015;37:348–53.

Decker T, Kovarik P. Serine phosphorylation of STATs. Oncogene 2000;19:2628–37.

Eriksen KW, Kaltoft K, Mikkelsen G, Nielsen M, Zhang Q, Geisler C, et al. Constitutive STAT3-activation in Sezary syndrome: tyrphostin AG490 inhibits STAT3-activation, interleukin-2 receptor expression and growth of leukemic Sezary cells. Leukemia 2001;15:787–93.

Fanok MH, Sun A, Fogli LK, Narendran V, Eckstein M, Kannan K, et al. Role of dysregulated cytokine signaling and bacterial triggers in the pathogenesis of cutaneous T-cell lymphoma. J Invest Dermatol 2018;138:1116–25.

Fantin VR, Loboda A, Paweletz CP, Hendrickson RC, Pierce JW, Roth JA, et al. Constitutive activation of signal transducers and activators of transcription predicts vorinostat resistance in cutaneous T-cell lymphoma. Cancer Res 2008;68:3785–94.

Gaydosik AM, Tabib T, Geskin LJ, Bayan CA, Conway JF, Lafyatis R, et al. Single-cell lymphocyte heterogeneity in advanced cutaneous T-cell lymphoma skin tumors. Clin Cancer Res 2019;25:4443–54.

Hamill S, Lou HJ, Turk BE, Boggon TJ. Structural basis for noncanonical substrate recognition of cofilin/ADF proteins by LIM kinases. Mol Cell 2016;62:397–408.

Isakov N, Altman A. Protein kinase C(theta) in T cell activation. Annu Rev Immunol 2002;20:761–94.

Iyer A, Hennessey D, O'Keefe S, Patterson J, Wang W, Salopek T, et al. Clonotypic heterogeneity in cutaneous T-cell lymphoma (mycosis fungoides) revealed by comprehensive whole-exome sequencing. Blood Adv 2019;3:1175–84.

Kamstrup MR, Gjerdrum LM, Biskup E, Lauenborg BT, Ralfkiaer E, Woetmann A, et al. Notch1 as a potential therapeutic target in cutaneous T-cell lymphoma. Blood 2010;116:2504–12.

Kiel MJ, Sahasrabuddhe AA, Rolland DCM, Velusamy T, Chung F, Schaller M, et al. Genomic analyses reveal recurrent mutations in epigenetic modifiers and the JAK-STAT pathway in Sézary syndrome. Nat Commun 2015;6:8470.

Kim EJ, Hess S, Richardson SK, Newton S, Showe LC, Benoit BM, et al. Immunopathogenesis and therapy of cutaneous T cell lymphoma [published correction appears in J Clin Invest 2007;117:836]. J Clin Invest 2005;115:798–812.

Klingenberg M, Becker J, Eberth S, Kube D, Wilting J. The chick chorioallantoic membrane as an in vivo xenograft model for Burkitt lymphoma. BMC Cancer 2014;14:339.

Lee EB, Fleischmann R, Hall S, Wilkinson B, Bradley JD, Gruben D, et al. Tofacitinib versus methotrexate in rheumatoid arthritis. N Engl J Med 2014;370:2377–86.

Malemud CJ. The role of the JAK/STAT signal pathway in rheumatoid arthritis [published correction appears in Ther Adv Musculoskelet Dis 2018;10:225]. Ther Adv Musculoskelet Dis 2018;10:117–27.

Mcgirt LY, Jia P, Baerenwald DA, Duszynski RJ, Dahlman KB, Zic JA, et al. Whole-genome sequencing reveals oncogenic mutations in mycosis fungoides. Blood 2015;126:508–19.

Meller N, Altman A, Isakov N. New perspectives on PKCtheta, a member of the novel subfamily of protein kinase C. Stem Cells 1998;16:178–92.

Mognol GP, Carneiro FR, Robbs BK, Faget DV, Viola JP. Cell cycle and apoptosis regulation by NFAT transcription factors: new roles for an old player. Cell Death Dis 2016;7:e2199.

Oka T, Miyagaki T. Novel and future therapeutic drugs for advanced mycosis fungoides and Sézary syndrome. Front Med (Lausanne) 2019;6:116.

Park J, Yang J, Wenzel AT, Ramachandran A, Lee WJ, Daniels JC, et al. Genomic analysis of 220 CTCLs identifies a novel recurrent gain-of-function alteration in RLTPR (p.Q575E). Blood 2017;130:1430–40.

Patel VM, Flanagan CE, Martins M, Jones CL, Butler RM, Woollard WJ, et al. Frequent and persistent PLCG1 mutations in Sézary cells directly enhance PLCγ1 activity and stimulate NFκB, AP-1, and NFAT signaling. J Invest Dermatol 2020;140:380–9.e4.

Pérez C, González-Rincón J, Onaindia A, Almaráz C, García-Díaz N, Pisonero H, et al. Mutated JAK kinases and deregulated STAT activity are potential therapeutic targets in cutaneous T-cell lymphoma. Haematologica 2015;100:e450–3.

Pérez C, Mondéjar R, García-Díaz N, Cereceda L, León A, Montes S, et al. Advanced-stage mycosis fungoides: role of the signal transducer and activator of transcription 3, nuclear factor-κB and nuclear factor of activated T cells pathways. Br J Dermatol 2020;182:147–55.

Prasad A, Rabionet R, Espinet B, Zapata L, Puiggros A, Melero C, et al. Identification of gene mutations and fusion genes in patients with Sézary syndrome. J Invest Dermatol 2016;136:1490–9.

Radine C, Peters D, Reese A, Neuwahl J, Budach W, Jänicke RU, et al. The RNA-binding protein RBM47 is a novel regulator of cell fate decisions by transcriptionally controlling the p53-p21-axis. Cell Death Differ 2020;27:1274–85.

Sakurai T, Isogaya K, Sakai S, Morikawa M, Morishita Y, Ehata S, et al. RNA-binding motif protein 47 inhibits Nrf2 activity to suppress tumor growth in lung adenocarcinoma [published correction appears in Oncogene 2017;36:5083]. Oncogene 2016;35:5000–9.

Sheren JE, Kassenbrock CK. RNF38 encodes a nuclear ubiquitin protein ligase that modifies p53. Biochem Biophys Res Commun 2013;440:473–8.

Sommer VH, Clemmensen OJ, Nielsen O, Wasik M, Lovato P, Brender C, et al. In vivo activation of STAT3 in cutaneous T-cell lymphoma. Evidence for an antiapoptotic function of STAT3. Leukemia 2004;18:1288–95.

Steinberg SF. Structural basis of protein kinase C isoform function. Physiol Rev 2008;88:1341–78.

Ungewickell A, Bhaduri A, Rios E, Reuter J, Lee CS, Mah A, et al. Genomic analysis of mycosis fungoides and Sézary syndrome identifies recurrent alterations in TNFR2. Nat Genet 2015;47:1056–60.

Vainchenker W, Constantinescu SN. JAK/STAT signaling in hematological malignancies. Oncogene 2013;32:2601–13.

Vaqué JP, Gómez-López G, Monsálvez V, Varela I, Martínez N, Pérez C, et al. PLCG1 mutations in cutaneous T-cell lymphomas. Blood 2014;123:2034–43.

Wang L, Ni X, Covington KR, Yang BY, Shiu J, Zhang X, et al. Genomic profiling of Sézary syndrome identifies alterations of key T cell signaling and differentiation genes. Nat Genet 2015;47:1426–34.

Willemze R, Jaffe ES, Burg G, Cerroni L, Berti E, Swerdlow SH, et al. WHO-EORTC classification for cutaneous lymphomas. Blood 2005;105:3768–85.

Willerslev-Olsen A, Krejsgaard T, Lindahl LM, Litvinov IV, Fredholm S, Petersen DL, et al. Staphylococcal enterotoxin A (SEA) stimulates STAT3 activation and IL-17 expression in cutaneous T-cell lymphoma. Blood 2016;127:1287–96.

Woollard WJ, Pullabhatla V, Lorenc A, Patel VM, Butler RM, Bayega A, et al. Candidate driver genes involved in genome maintenance and DNA repair in Sézary syndrome. Blood 2016;127:3387–97.

SUPPLEMENTARY MATERIALS AND METHODS

Cell culture

Human HuT 78, Jurkat, and HH cell lines were obtained from ATCC (Rockville, MD). The human MyLa cell line was obtained from the European Collection of Cell Cultures (Salisbury, United Kingdom). They were cultured in RPMI-1640 medium supplemented with 10% heat-inactivated fetal bovine serum (Gibco, Thermo Fisher Scientific, Waltham, MA). HEK293 (ATCC) and HEK-Blue IL-6 cells (HEK-IL6, InvivoGen, San Diego, CA) were cultured in DMEM medium supplemented with 10% fetal bovine serum, and the latter were also supplemented with 100 μg/ml Normocin, 200 μg/ml Hygromycin B Gold, and 100 μg/ml Zeocin (InvivoGen). All cell lines were supplemented with glucose (4.5 g/l), L-glutamine (292 mg/l), streptomycin sulfate (10 mg/l), and potassium penicillin (10,000 U/l) (Lonza, Basel, Switzerland) and maintained in a humidified atmosphere at 37 °C and 5% carbon dioxide.

Reagents and plasmid constructs

Tacrolimus, sotrastaurin, and ruxolitinib inhibitors were obtained from Selleckchem, Germany. 12-*O*-tetradecanoylphorbol-13-acetate and IL-6 (P1585 and SRP3096, respectively) were obtained from Sigma-Aldrich (St. Louis, MO).

Empty vector and PLCG1 constructs are described elsewhere (Vaqué et al., 2014). Human PRKCQ ORF clone (pCMV6-Entry-PRKCQ Myc-DDK-tagged, RC210910; Origene Technologies, Rockville, MD) was subjected to mutagenesis using QuickChange Lightning Site-Directed Mutagenesis Kit (Agilent Technologies, Santa Clara, CA), following the manufacturer's instructions. The mutagenic and confirmation primer sequences are listed in Supplementary Table S1.

Determination of STAT3 activity

Quanti-Blue, luciferase reporter, and TransAM transcription factor assays were used to analyze signal transducer and activator of transcription (STAT) 3 activity in MyLa, HuT 78, HEK293, and HEK-IL6 cells. Briefly, the Quanti-Blue assay determines the activity of secreted embryonic alkaline phosphatase fused to four STAT3 binding sites (STAT3-SEAP). HEK-IL6 cells were cultured in six-well plates and treated under the desired conditions. Then, 20 μl of the supernatant were incubated at 37 °C with 180 μl of Quanti-Blue solution in a 96-well flat plate for 90 minutes. SEAP levels were quantified at 620−655 nm on a Spark Multimode Microplate Reader (Tecan Trading AG, Switzerland).

A luciferase report assay was performed in HEK293 cells using Dual-Glo Luciferase Assay System (Promega, Madison, WI). Cells were seeded in 12-well plates and, 24 hours later, transiently transfected with Lipofectamine LTX and PLUS reagents (Invitrogen, Waltham, MA) with a mix of DNA plasmids specific for each experiment. General conditions were 0.3 μg of firefly STAT3 luciferase reporter (pGL4.47 vector, Promega), 0.1 μg of pRL-Null *Renilla* luciferase control reporter vector (Promega), and 1 μg of the specific gene or control constructs used for each experiment. Cells without transfected DNA plasmids were used as a blank. At 48 hours after transfection, passive lysis and quantification of *Renilla* and firefly levels were performed following the manufacturer's instructions. Luminescence was measured with a GloMax-Multi reader (Promega).

To detect and quantify the capacity of activated STAT3 to bind to its DNA consensus binding sites in HuT 78 cells, an ELISA-based assay was performed using a TransAM STAT3 transcription factor assay kit (Active Motif, Carlsbad, CA) following the manufacturer's instructions. Nuclear proteins of cells treated under desired conditions were lysed using a Nuclear Extract Kit (Active Motif) following the manufacturer's instructions. Finally, absorbance was read on a Spark Multimode Microplate Reader (Tecan Trading AG) at 450 nm with an optimal reference wavelength of 655 nm. Wells without nuclear proteins were used as a blank.

Western blot

Cells were starved overnight, treated under the desired conditions, and lysed with RIPA buffer (Sigma-Aldrich) supplemented with phosphatase and protease inhibitors (Roche, Basel, Switzerland). Whole-cell lysates were subjected to acrylamide SDS-PAGE using standard procedures, transferred onto a nitrocellulose support membrane (GE Healthcare, Chicago, IL), and western blotted. The following antibodies were used: α Tubulin (Santa Cruz Biotechnology, Dallas, TX); FLAG (DDK, Origene Technologies); phospho-STAT3 Y705, phospho-STAT3 S727, STAT3, and protein kinase C θ (Cell Signaling, Danvers, MA); and goat anti-mouse IgG DyLight 800 and goat anti-rabbit IgG Dylight 680 (Invitrogen). Bands were visualized and recorded with an Odyssey Infrared Imaging scanner (LI-COR Biosciences, Lincoln, NE) and were quantified by densitometry using Image Studio Software (LI-COR Biosciences).

Generation of PRKCQ knockdown cell lines

Protein kinase C θ expression was knocked down by stably transducing lentiviral particles carrying turboGFP and doxycycline-inducible nontargeting control short hairpin RNA (shRNA) or shRNA against human PRKCQ mRNA (Dharmacon, Lafayette, CO) in MyLa, HuT 78, Jurkat, and HEK-IL6 cells. Lentiviral particles were produced by cotransfection of 293T cells using the Trans-Lentiviral shRNA Packaging System (Dharmacon) following the manufacturer's instructions. Unless otherwise stated, cells were incubated with doxycycline (1 μg/ml, Sigma-Aldrich) for 72 hours to induce GFP and shRNA expression. Transfected cells were selected with puromycin (1 μg/ml, Sigma-Aldrich) for at least 7 days.

Drug synergism assays

To assess drug synergism and generate combination index (CI) values, CalcuSyn software (Biosoft, Cambridge, United Kingdom) was used as previously described (Chou and Talalay, 1984). This determines whether a combination of two drugs produces a synergistic ($CI < 1$), additive ($CI = 1$), or antagonistic effect ($CI > 1$), evaluating the fraction of affected cells (cell viability) of each inhibitor alone compared with the combination of inhibitors.

Cell viability and apoptosis assays

Cell proliferation was measured as the intracellular ATP content using the CellTiter-Glo Luminescent Cell Viability Assay kit (Promega) following the manufacturer instructions, and luminometric changes were quantified using the Synergy

HTX Multi-Mode Microplate Reader (BioTek, Winooski, VT). The half maximal inhibitory concentration was estimated after 48 hours of drug treatment using GraphPad Prism software (GraphPad Sotfware, San Diego, CA). Cell proliferation, analyzed in nontargeting control or shRNA *PRKCQ* MyLa and HuT 78 cells, was performed after incubation with doxycycline for 72 hours.

Induction of apoptosis was evaluated using a FlowCellect Annexin Red Kit (Merck Millipore, Burlington, MA) according to the manufacturer's instructions. Data were collected using a CytoFLEX flow cytometer and analyzed with CytExpert software (Beckman Coulter, Brea, CA).

Immunohistochemical analysis

Immunohistochemical expression of H&E, CD30, and phospho-STAT3 Y705 was assessed using routine immunohistochemical techniques for primary tumors from chicken embryos. Estimation of the percentage of tumoral cells in patient samples, both in H&E and immunohistochemistry, of every case studied was determined. The proportion of atypical cells among the infiltrate was calculated considering the percentage of cells with large atypical nuclei and the CD4 (or CD8 in selected cases) with loose of pan-T markers.

RT-qPCR

cDNA synthesis was performed using the SuperScript IV Reverse Transcriptase (Invitrogen). cDNA was amplified using the Power SYBR Green PCR Master Mix in a 7300 Fast Real-Time PCR System (Applied Biosystems, Waltham, MA). Specific oligos were designed using Primer-Blast (NCBI). *ACTB* expression was used to normalize values. Gene expression changes were determined using $2^{(-\Delta\Delta Ct)}$ formula. A melting curve was generated for every run to confirm assay specificity.

RNA-sequencing analysis

High-quality total RNA (RNA integrity number $>$ 8) was isolated using TRIzol reagent (Invitrogen) following the manufacturer's instructions. The RNA-sequencing libraries were prepared following the TruSeq Stranded mRNA LT Sample Prep Kit protocol (Illumina, San Diego, CA). Briefly, total RNA (500 ng) was enriched for the polyA mRNA fraction and fragmented by divalent metal cations at high temperature. To achieve directionality, second-strand cDNA synthesis was performed in the presence of dUTP. The blunt-ended double-stranded cDNA was 3′-adenylated, and Illumina platform-compatible adaptors with Unique Dual Indexes and Unique Molecular Identifiers (Integrated DNA Technologies, Coralville, IA) were ligated. The ligation product was enriched with 15 PCR cycles and the final library was validated on an Agilent 2100 Bioanalyzer with the DNA 7500 assay (Agilent Technologies). The libraries were sequenced in a HiSeq4000 (Illumina) following the manufacturer's protocol for dual indexing. Image analysis, base calling, and quality scoring of the run were carried out using the manufacturer's Real Time Analysis (RTA 2.7.7) software, after which FASTQ sequence files were generated. RNA-sequencing paired-end reads were mapped against the human reference genome (GRCh38) using STAR version 2.5.3a (Dobin et al., 2013) with ENCODE parameters for long RNA. Annotated genes (GENCODE version 29) were quantified using RSEM version 1.3.0 with default parameters (Li and Dewey, 2014). Differential expression was analyzed with DESeq2 version 1.18.1 (Love et al., 2014). Gene set enrichment analysis was performed to identify significantly altered gene pathways (Mootha et al., 2003; Subramanian et al., 2005).

SUPPLEMENTARY REFERENCES

Chou TC, Talalay P. Quantitative analysis of dose-effect relationships: the combined effects of multiple drugs or enzyme inhibitors. Adv Enzyme Regul 1984;22(C):27–55.

Dobin A, Davis CA, Schlesinger F, et al. STAR: ultrafast universal RNA-seq aligner. Bioinformatics 2013;29:15–21.

Li B, Dewey CN. RSEM: accurate transcript quantification from RNA-seq data with or without a reference genome. Bioinforma Impact Accurate Quantif Proteomic Genet Anal Res 2014:41–74.

Love MI, Huber W, Anders S. Moderated estimation of fold change and dispersion for RNA-seq data with DESeq2. Genome Biol 2014;15:550.

Mootha VK, Lindgren CM, Eriksson KF, et al. PGC-1α-responsive genes involved in oxidative phosphorylation are coordinately downregulated in human diabetes. Nat. Genet 2003;34:267–73.

Subramanian A, Tamayo P, Mootha VK, et al. Gene set enrichment analysis: a knowledge-based approach for interpreting genome-wide expression profiles. Proc Natl Acad Sci U S A 2005;102:15545–50.

Vaqué JP, Gómez-López G, Monsálvez V, et al. PLCG1 mutations in cutaneous T-cell lymphomas. Blood 2014;123:2034–44.

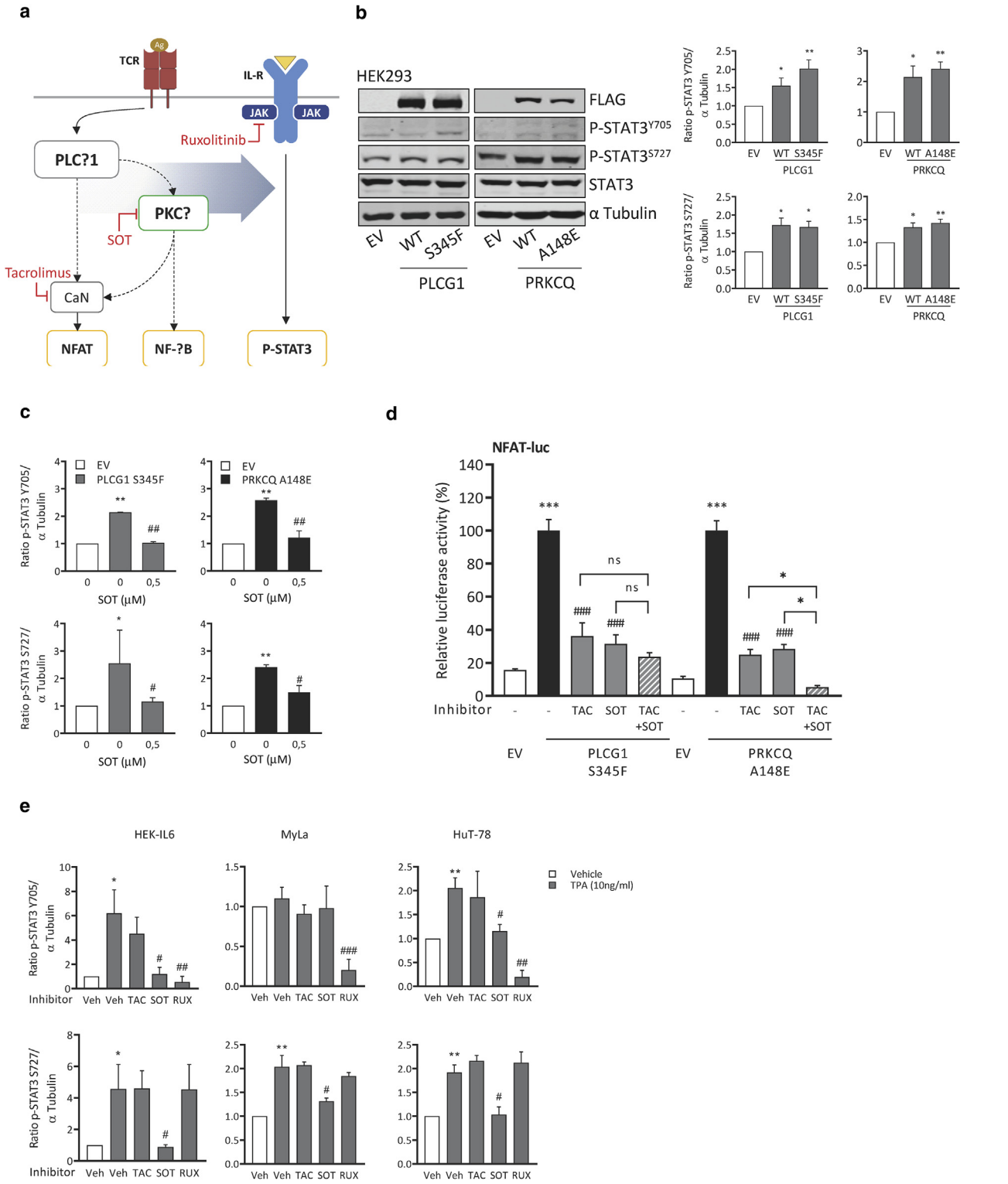

Supplementary Figure S1. PLCγ1/PKCθ activates STAT3 and NFAT. (**a**) Schematic representation of the signaling network mediated by PLCγ1 and PKCθ toward NFAT, NF-κB, and STAT transcription factors. (**b**) Western blot of HEK293 cells transiently transfected with the indicated vectors, starved, and incubated with the indicated antibodies, and quantification of three independent blots by densitometry using Image Studio Software (P-Y705 and P-S727 STAT3 relative to α tubulin from each blot). Quantification of three independent blots from Figure 1b (**c**) and Figure 1c (**e**) by densitometry. (**d**) NFAT luciferase reporter activity in HEK293 cells transfected with the indicated vectors and treated with the indicated inhibitors (1 μM, 24 hours, n = 3). Images are representative of each western blot (n = 3). Data are mean ± SEM. Student's *t*-test: $*P < 0.05$, $**P < 0.01$, and $***P < 0.001$ versus EV (**b**–**d**) or vehicle (**e**); $\#P < 0.05$, $\#\#P < 0.01$, and $\#\#\#P < 0.001$ versus PLCG1 S345F or PRKCQ A148E treated with control vehicle (**c, d**), or TPA (**e**). CaN, calcineurin; EV, empty vector; ns, not significant; PKC, protein kinase C; P-STAT, phosphorylated signal transducer and activator of transcription; RUX, ruxolitinib; SOT, sotrastaurin; STAT, signal transducer and activator of transcription; TAC, tacrolimus; TPA, 12-*O*-tetradecanoylphorbol-13-acetate; Veh, vehicle; WT, wild type.

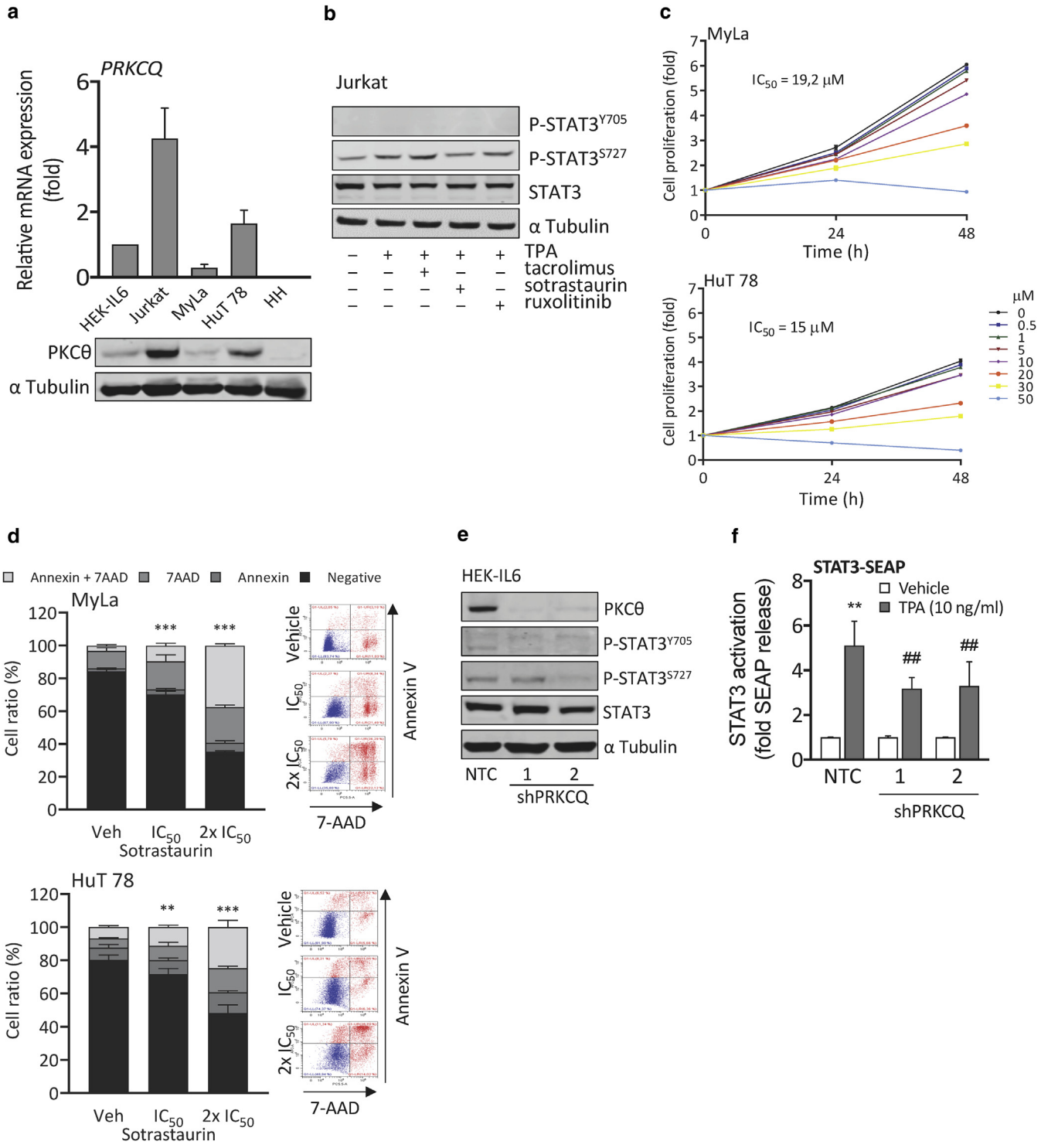

Supplementary Figure S2. PKCθ inhibition impairs STAT3 activation and proliferation, and induce apoptosis in CTCL cells. (**a**) mRNA expression levels (top) and protein expression (bottom) of *PRKCQ*/PKCθ in HEK-IL6, Jurkat, MyLa, HuT 78, and HH cells. (**b**) Western blot analyses of starved Jurkat cells treated with the indicated inhibitors (1 μM, 3 hours) and TPA (10 ng/ml, 1 hours) and incubated with the indicated antibodies. (**c**) Proliferation analyses in MyLa and HuT 78 cells treated with increasing concentrations of sotrastaurin at 0, 24, and 48 hours. (**d**) Percentage of early (Annexin V) or late (7-AAD) apoptotic MyLa and HuT 78 cells incubated with sotrastaurin (24 hours, n = 3). Representative plots of Annexin V (Y axis) and 7-AAD (X axis) staining data of each condition are shown. Student *t*-test: comparison between viable cells (negative staining) treated with sotrastaurin and viable cells treated with control vehicle. (**e**) Western blot analyses of inducible NTC or shPRKCQ HEK-IL6 cells incubated with the indicated antibodies. (**f**) Quantification of SEAP release in NTC and shPRKCQ HEK-IL6 cells treated with TPA (10 ng/ml overnight, n = 3). Images are representative of each western blot. Data are mean ± SEM. Student's *t*-test: $^{**}P < 0.01$ versus NTC treated with vehicle (f); $^{\#\#}P < 0.01$ versus NTC treated with TPA (f). CTCL, cutaneous T-cell lymphoma; IC_{50}, half maximal inhibitory concentration; NTC, nontargeting control; PKC, protein kinase C; P-STAT, phosphorylated signal transducer and activator of transcription; shPRKCQ, *PRKCQ* short hairpin RNA; STAT, signal transducer and activator of transcription; TPA, 12-*O*-tetradecanoylphorbol-13-acetate.

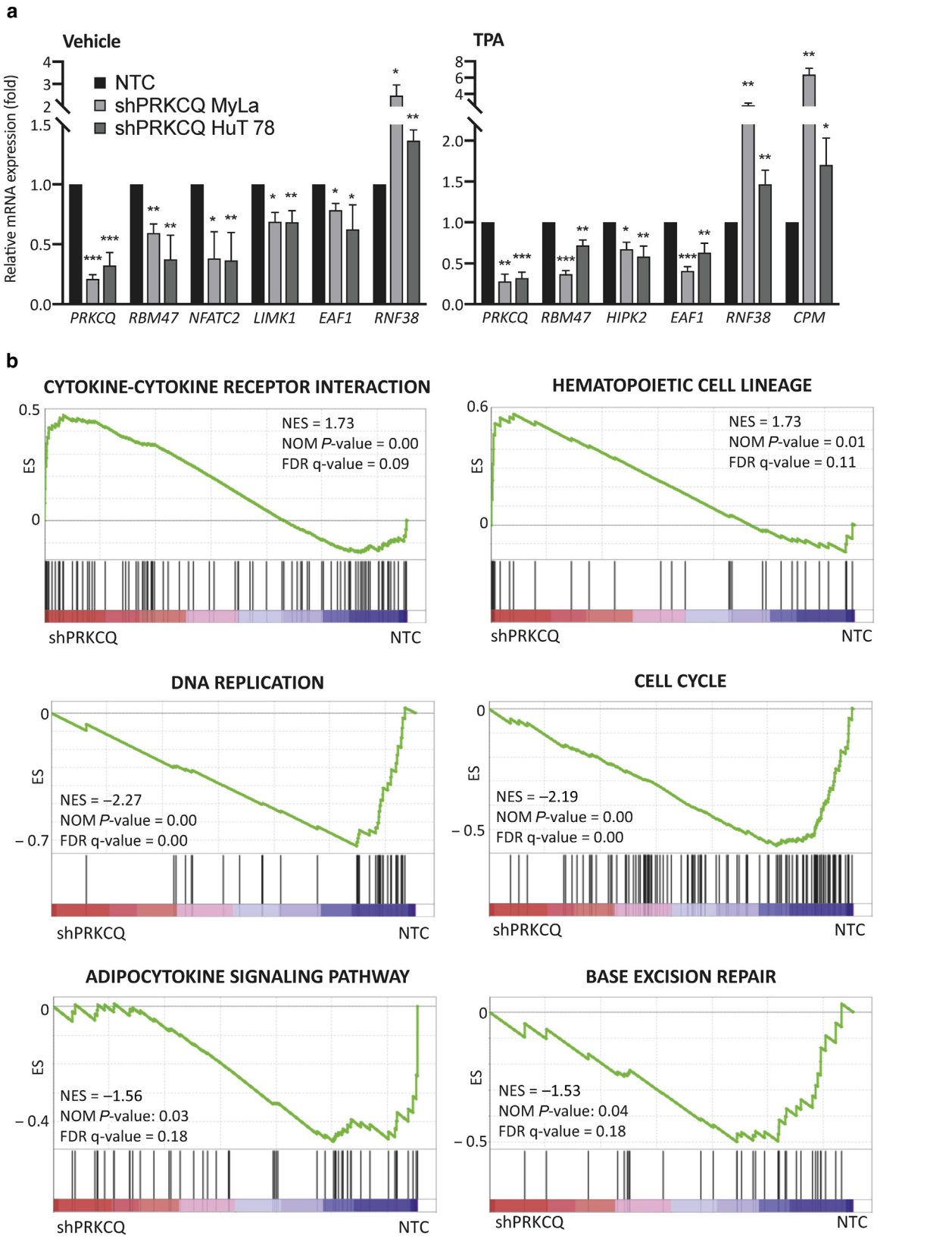

Supplementary Figure S3. PKCθ target genes and pathways in CTCL cells. (**a**) mRNA expression levels of the indicated genes in shPRKCQ MyLa and HuT 78 cells compared with NTC cells treated with control vehicle or TPA (10 ng/ml, 24 hours). (**b**) Selected GSEA plots shared in shPRKCQ MyLa and HuT 78 cells compared with NTC cells (see Supplementary Table S2 for a complete list of GSEA signatures). Gene sets with a NOM *P*-value < 0.05 and FDR q-value < 0.25 were considered significantly enriched. Data are mean ± SEM (n = 3). Student's *t*-test: $*P < 0.05$, $**P < 0.01$, and $***P < 0.001$ versus NTC. CTCL, cutaneous T-cell lymphoma; FDR q-value, false discovery rate q-value; GSEA, gene set enrichment analysis; NES, normalized enrichment score; NOM *P*-value, nominal *P*-value; NTC, nontargeting control; PKC, protein kinase C; shPRKCQ, *PRKCQ* short hairpin RNA; TPA, 12-*O*-tetradecanoylphorbol-13-acetate.

Supplementary Figure S4. Pharmacological and genetic inhibition of PKCθ reduces P-STAT3 in vivo. (**a**) Representative images of control and shPRKCQ chicken embryos. Primary tumor is rounded with a dashed circle. (**b**) H&E and P-STAT3 Y705 staining of paraffin sections of control, tumors treated once or twice with sotrastaurin, and tumors with PKCθ deficiency (shPRKCQ). Bar = 100 μm. PKC, protein kinase C; P-STAT, phosphorylated signal transducer and activator of transcription; shPRKCQ, *PRKCQ* short hairpin RNA; STAT, signal transducer and activator of transcription.

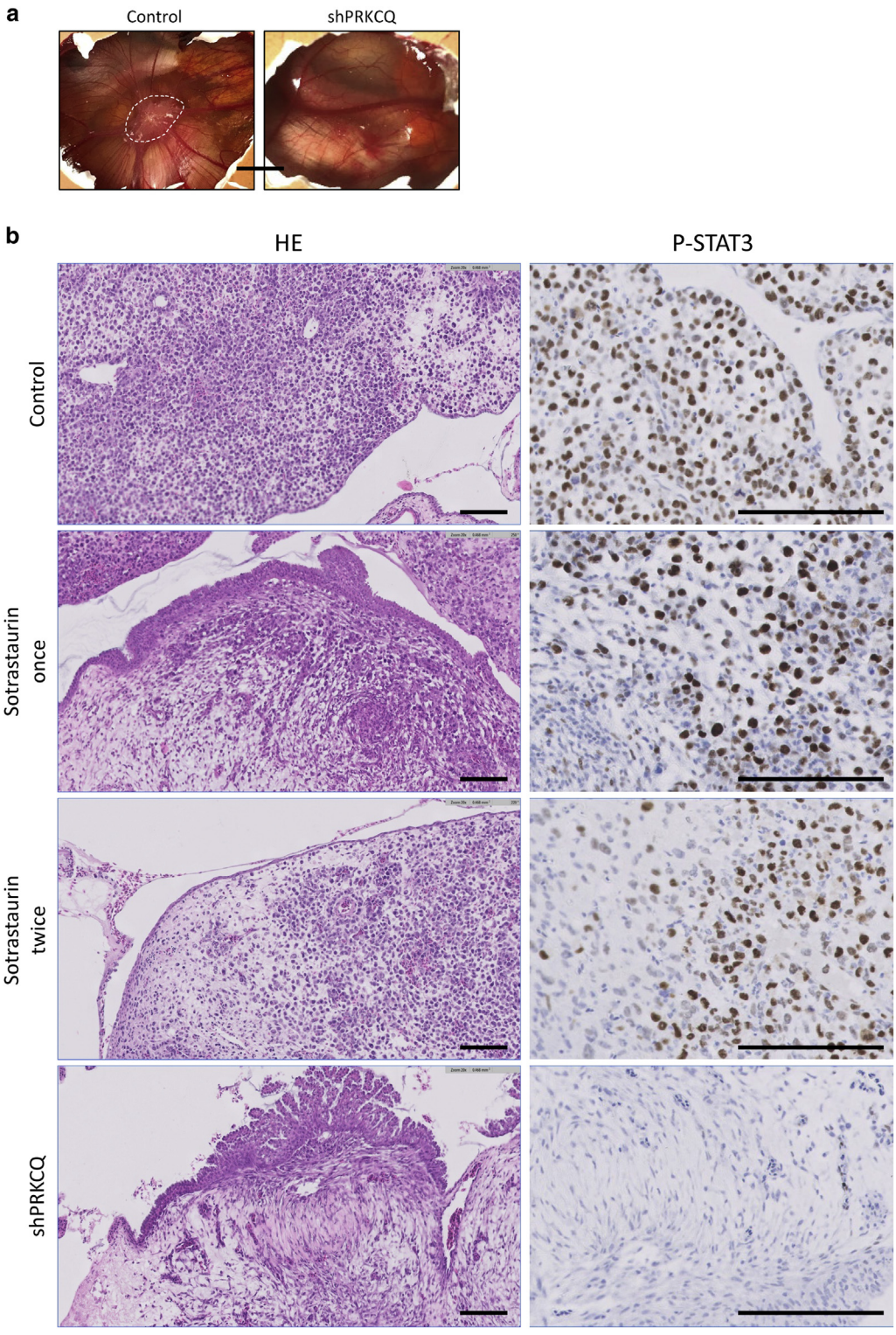

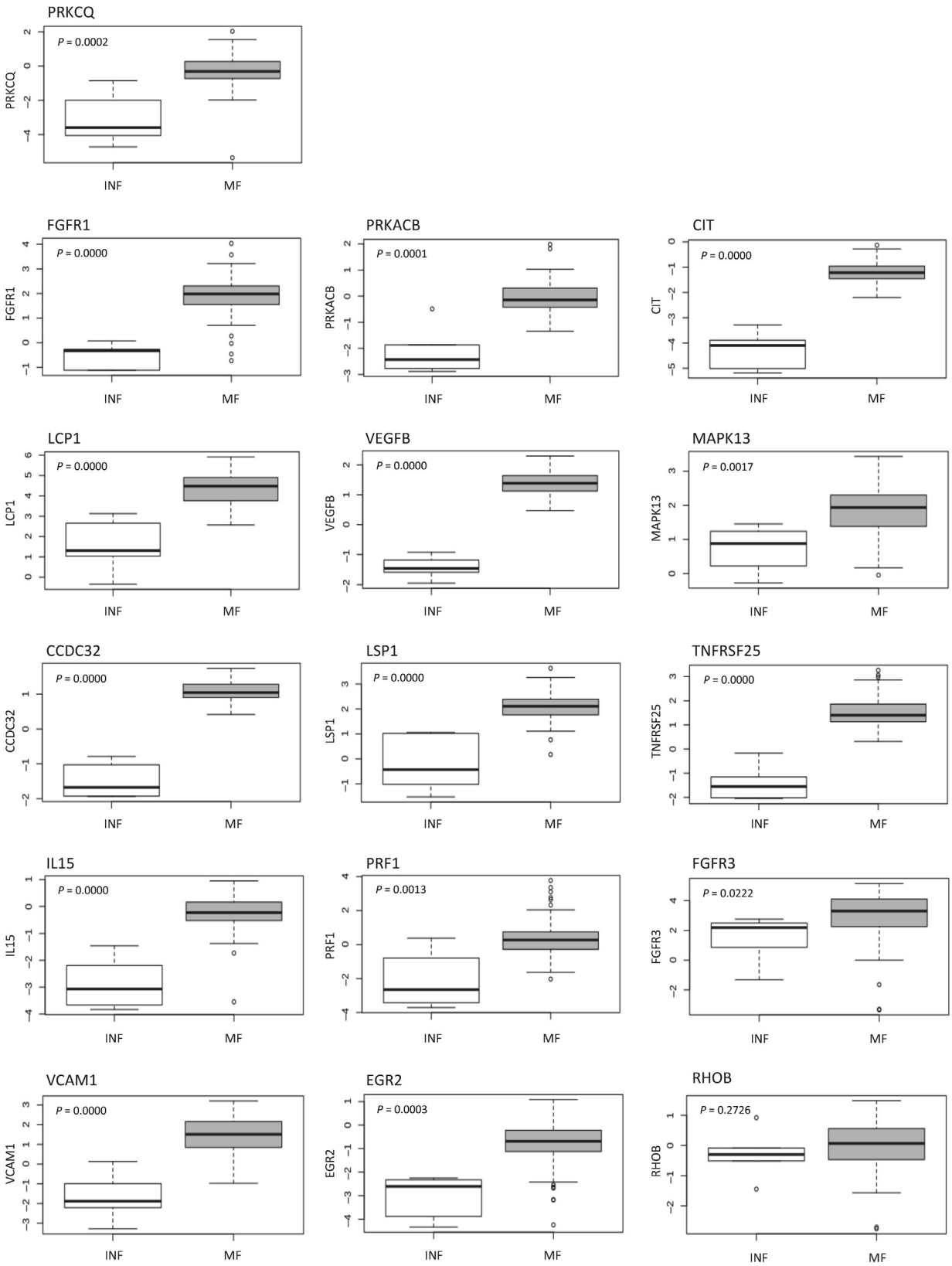

Supplementary Figure S5. Expression of PRKCQ and its target genes in MF versus inflammatory controls. Box plots showing the expression of PRKCQ and its target genes in six samples of inflammatory dermatoses and 81 samples of patients with MF. INF, inflammatory dermatoses; MF, mycosis fungoides.

Supplementary Table S1. Primer Sequences Used in this Work

Name	Forward 5′-3′ Sequence	Reverse 5′-3′ Sequence
PRKCQ-A148E mutagenesis	CTTTGCCTGCTTGATCTCACCCCGGCGCTGAT	ATCAGCGCCGGGGTGAGATCAAGCAGGCAAAG
PRKCQ-K409R mutagenesis	CATCTTTCTTTAAGGCCCTTATTGCGAAAAATTGATTGG TTTTCTTGAATT	AATTCAAGAAAACCAATCAATTTTTCGCAATAA GGGCCTTAAAGAAAGATG
PRKCQ-A148E confirmation	ACTTTCTGGAAATGAGTGACACAA	ATGTGGGCTGTGGGAAGAAG
PRKCQ-K409R confirmation	TGGGGAAAGGAAGTTTTGGCA	TCCCAGGCCAAGGAAAGAAC
Alu	ACGCCTGTAATCCCAGGACTT	TCGCCCAGGCTGGCTGGGTGCA
GAPDH (Chicken)	GAGGAAAGGTCGCCTGGTGGATCG	GGTGAGGACAAGCAGTGAGGAACG
PRKCQ	CCATGTCGCCATTTCTTCGG	GCCCGTTCTCTGATTCGACA
RBM47	CAGCCATGAGCAGTGACTCG	TCTTGCACCATGCTGTAGCC
NFATC2	GTATTACCTGCGGGGGTGAC	TCTGATTTCTGGCAGGAGGTC
LIMK1	ACGCTACTTTGTTGCACCTG	ATCATAGATCCTCTGGCCGC
EAF1	GGGCCTCCTTCCACACTATT	GCCGTTTGTTCCCCTTGAAC
NOTCH1	GAATGGCGGGAAGTGTGAAGC	TAGTCTGCCACGCCTCTGC
RNF38	GGTGAGACTTCAGAGCCTGTT	GAGAGAGGCGCTGTCTCTTAG
HIPK2	CCCATCTACACTCTACCAGCC	GAGTAGCCAGCGTGCTTAGA
CPM	CAGGAAGGGATGGAAGCGTT	GTGTTCCTTTGGAAACCGCC
ACTB	AGTGTGACGTGGACATCCGCAAAG	ATCCACATCTGCTGGAAGGTGGAC

Supplementary Table S2. GSEA Data

Positively Deregulated DMSO

	Gene Set	NES	NOM *P*-Value	FDR q-Value	FWER *P*-Value
1	KEGG_RIBOSOME	1.870	0.000	0.114	0.122
2	KEGG_SYSTEMIC_LUPUS_ERYTHEMATOSUS	1.810	0.006	0.115	0.232
3	KEGG_COMPLEMENT_AND_COAGULATION_CASCADES	1.760	0.013	0.117	0.330
4	KEGG_HEMATOPOIETIC_CELL_LINEAGE	1.730	0.011	0.116	0.419
5	KEGG_CYTOKINE_CYTOKINE_RECEPTOR_INTERACTION	1.730	0.000	0.097	0.429
6	KEGG_ALDOSTERONE_REGULATED_SODIUM_REABSORPTION	1.570	0.034	0.270	0.846
7	KEGG_BASAL_CELL_CARCINOMA	1.560	0.030	0.250	0.868
8	KEGG_ANTIGEN_PROCESSING_AND_PRESENTATION	1.540	0.026	0.249	0.913
9	KEGG_PARKINSONS_DISEASE	1.540	0.011	0.222	0.913
10	KEGG_CHEMOKINE_SIGNALING_PATHWAY	1.490	0.009	0.271	0.955
11	KEGG_SPLICEOSOME	1.490	0.008	0.253	0.956
12	KEGG_OXIDATIVE_PHOSPHORYLATION	1.470	0.015	0.275	0.977
13	KEGG_PATHOGENIC_ESCHERICHIA_COLI_INFECTION	1.440	0.052	0.299	0.987
14	KEGG_THYROID_CANCER	1.360	0.108	0.424	1.000
15	KEGG_TOLL_LIKE_RECEPTOR_SIGNALING_PATHWAY	1.350	0.068	0.429	1.000
16	KEGG_ALZHEIMERS_DISEASE	1.300	0.064	0.532	1.000
17	KEGG_HUNTINGTONS_DISEASE	1.290	0.075	0.537	1.000
18	KEGG_REGULATION_OF_AUTOPHAGY	1.280	0.161	0.513	1.000
19	KEGG_PROTEASOME	1.270	0.124	0.513	1.000
20	KEGG_GLYCOSAMINOGLYCAN_BIOSYNTHESIS_HEPARAN_SULFATE	1.240	0.200	0.563	1.000
21	KEGG_ARRHYTHMOGENIC_RIGHT_VENTRICULAR_CARDIOMYOPATHY	1.230	0.207	0.581	1.000
22	KEGG_FOCAL_ADHESION	1.180	0.161	0.681	1.000
23	KEGG_GLYCOSAMINOGLYCAN_BIOSYNTHESIS_CHONDROITIN_SULFATE	1.140	0.297	0.770	1.000
24	KEGG_HEDGEHOG_SIGNALING_PATHWAY	1.110	0.312	0.831	1.000
25	KEGG_MAPK_SIGNALING_PATHWAY	1.110	0.214	0.805	1.000
26	KEGG_GLYCOLYSIS_GLUCONEOGENESIS	1.090	0.345	0.843	1.000
27	KEGG_HYPERTROPHIC_CARDIOMYOPATHY_HCM	1.080	0.309	0.846	1.000
28	KEGG_ENDOMETRIAL_CANCER	1.080	0.352	0.834	1.000
29	KEGG_VIRAL_MYOCARDITIS	1.070	0.353	0.822	1.000
30	KEGG_GAP_JUNCTION	1.070	0.365	0.802	1.000

(*continued*)

Supplementary Table S2. Continued

Positively Deregulated DMSO

	Gene Set	NES	NOM *P*-Value	FDR q-Value	FWER *P*-Value
31	KEGG_PRIMARY_IMMUNODEFICIENCY	1.060	0.375	0.808	1.000
32	KEGG_ERBB_SIGNALING_PATHWAY	1.050	0.363	0.804	1.000
33	KEGG_RENAL_CELL_CARCINOMA	1.050	0.375	0.788	1.000
34	KEGG_SNARE_INTERACTIONS_IN_VESICULAR_TRANSPORT	1.040	0.418	0.786	1.000
35	KEGG_PATHWAYS_IN_CANCER	1.020	0.395	0.805	1.000
36	KEGG_REGULATION_OF_ACTIN_CYTOSKELETON	1.020	0.402	0.793	1.000
37	KEGG_ECM_RECEPTOR_INTERACTION	1.010	0.425	0.798	1.000
38	KEGG_NEUROTROPHIN_SIGNALING_PATHWAY	0.990	0.470	0.843	1.000
39	KEGG_ARACHIDONIC_ACID_METABOLISM	0.980	0.478	0.837	1.000
40	KEGG_NATURAL_KILLER_CELL_MEDIATED_CYTOTOXICITY	0.980	0.470	0.822	1.000
41	KEGG_COLORECTAL_CANCER	0.960	0.514	0.847	1.000
42	KEGG_GLYCOSAMINOGLYCAN_DEGRADATION	0.930	0.543	0.924	1.000
43	KEGG_EPITHELIAL_CELL_SIGNALING_IN_H_PYLORI_INFECTION	0.930	0.573	0.905	1.000
44	KEGG_RNA_DEGRADATION	0.900	0.614	0.940	1.000
45	KEGG_RIG_I_LIKE_RECEPTOR_SIGNALING_PATHWAY	0.880	0.653	0.971	1.000
46	KEGG_NEUROACTIVE_LIGAND_RECEPTOR_INTERACTION	0.880	0.637	0.966	1.000
47	KEGG_CARDIAC_MUSCLE_CONTRACTION	0.880	0.653	0.948	1.000
48	KEGG_FRUCTOSE_AND_MANNOSE_METABOLISM	0.840	0.690	1.000	1.000
49	KEGG_ENDOCYTOSIS	0.810	0.847	1.000	1.000
50	KEGG_P53_SIGNALING_PATHWAY	0.800	0.804	1.000	1.000
51	KEGG_BETA_ALANINE_METABOLISM	0.780	0.731	1.000	1.000
52	KEGG_BLADDER_CANCER	0.770	0.797	1.000	1.000
53	KEGG_FC_EPSILON_RI_SIGNALING_PATHWAY	0.760	0.841	1.000	1.000
54	KEGG_PHOSPHATIDYLINOSITOL_SIGNALING_SYSTEM	0.750	0.868	1.000	1.000
55	KEGG_NUCLEOTIDE_EXCISION_REPAIR	0.750	0.862	1.000	1.000
56	KEGG_GLUTATHIONE_METABOLISM	0.750	0.836	1.000	1.000
57	KEGG_GLYCEROLIPID_METABOLISM	0.720	0.867	1.000	1.000
58	KEGG_PORPHYRIN_AND_CHLOROPHYLL_METABOLISM	0.710	0.835	1.000	1.000
59	KEGG_LEISHMANIA_INFECTION	0.700	0.917	1.000	1.000
60	KEGG_PROGESTERONE_MEDIATED_OOCYTE_MATURATION	0.690	0.942	1.000	1.000
61	KEGG_BASAL_TRANSCRIPTION_FACTORS	0.680	0.881	1.000	1.000
62	KEGG_CHRONIC_MYELOID_LEUKEMIA	0.680	0.941	1.000	1.000
63	KEGG_RNA_POLYMERASE	0.660	0.916	1.000	1.000
64	KEGG_BASE_EXCISION_REPAIR	0.650	0.936	1.000	1.000
65	KEGG_ACUTE_MYELOID_LEUKEMIA	0.630	0.965	0.998	1.000
66	KEGG_PROTEIN_EXPORT	0.620	0.928	0.989	1.000
67	KEGG_UBIQUITIN_MEDIATED_PROTEOLYSIS	0.620	0.998	0.975	1.000
68	KEGG_MTOR_SIGNALING_PATHWAY	0.560	0.991	0.983	1.000

Negatively Deregulated DMSO

	Gene Set	NES	NOM *P*-Value	FDR q-Value	FWER *P*-Value
1	KEGG_GLYCINE_SERINE_AND_THREONINE_METABOLISM	−1.550	0.055	1.000	0.849
2	KEGG_ABC_TRANSPORTERS	−1.550	0.046	1.000	0.850
3	KEGG_ADIPOCYTOKINE_SIGNALING_PATHWAY	−1.490	0.031	1.000	0.952
4	KEGG_AMINO_SUGAR_AND_NUCLEOTIDE_SUGAR_METABOLISM	−1.420	0.051	1.000	0.991
5	KEGG_VASCULAR_SMOOTH_MUSCLE_CONTRACTION	−1.400	0.057	1.000	0.997
6	KEGG_CITRATE_CYCLE_TCA_CYCLE	−1.390	0.090	0.999	0.997
7	KEGG_NOTCH_SIGNALING_PATHWAY	−1.390	0.087	0.877	0.998
8	KEGG_STEROID_BIOSYNTHESIS	−1.390	0.115	0.771	0.998
9	KEGG_LYSOSOME	−1.380	0.041	0.712	0.998
10	KEGG_MELANOMA	−1.380	0.064	0.651	0.998
11	KEGG_VASOPRESSIN_REGULATED_WATER_REABSORPTION	−1.370	0.101	0.605	0.999
12	KEGG_AUTOIMMUNE_THYROID_DISEASE	−1.360	0.139	0.615	0.999
13	KEGG_LONG_TERM_POTENTIATION	−1.340	0.092	0.635	1.000
14	KEGG_CELL_ADHESION_MOLECULES_CAMS	−1.330	0.079	0.599	1.000
15	KEGG_PPAR_SIGNALING_PATHWAY	−1.330	0.128	0.570	1.000
16	KEGG_CALCIUM_SIGNALING_PATHWAY	−1.290	0.080	0.659	1.000

(*continued*)

Supplementary Table S2. Continued

Negatively Deregulated DMSO

	Gene Set	NES	NOM *P*-Value	FDR q-Value	FWER *P*-Value
17	KEGG_SELENOAMINO_ACID_METABOLISM	−1.280	0.164	0.663	1.000
18	KEGG_DORSO_VENTRAL_AXIS_FORMATION	−1.260	0.174	0.665	1.000
19	KEGG_GNRH_SIGNALING_PATHWAY	−1.250	0.158	0.671	1.000
20	KEGG_PROPANOATE_METABOLISM	−1.250	0.201	0.659	1.000
21	KEGG_ONE_CARBON_POOL_BY_FOLATE	−1.240	0.203	0.633	1.000
22	KEGG_ALLOGRAFT_REJECTION	−1.210	0.218	0.708	1.000
23	KEGG_TYPE_I_DIABETES_MELLITUS	−1.200	0.218	0.712	1.000
24	KEGG_AXON_GUIDANCE	−1.190	0.162	0.710	1.000
25	KEGG_VIBRIO_CHOLERAE_INFECTION	−1.180	0.223	0.709	1.000
26	KEGG_GALACTOSE_METABOLISM	−1.180	0.262	0.684	1.000
27	KEGG_PROSTATE_CANCER	−1.150	0.242	0.758	1.000
28	KEGG_TRYPTOPHAN_METABOLISM	−1.140	0.282	0.747	1.000
29	KEGG_N_GLYCAN_BIOSYNTHESIS	−1.140	0.251	0.725	1.000
30	KEGG_ALANINE_ASPARTATE_AND_GLUTAMATE_METABOLISM	−1.120	0.310	0.762	1.000
31	KEGG_T_CELL_RECEPTOR_SIGNALING_PATHWAY	−1.110	0.263	0.765	1.000
32	KEGG_GRAFT_VERSUS_HOST_DISEASE	−1.110	0.340	0.743	1.000
33	KEGG_TIGHT_JUNCTION	−1.110	0.265	0.726	1.000
34	KEGG_LONG_TERM_DEPRESSION	−1.100	0.316	0.733	1.000
35	KEGG_STARCH_AND_SUCROSE_METABOLISM	−1.090	0.342	0.735	1.000
36	KEGG_WNT_SIGNALING_PATHWAY	−1.070	0.316	0.791	1.000
37	KEGG_PRION_DISEASES	−1.050	0.405	0.830	1.000
38	KEGG_CYTOSOLIC_DNA_SENSING_PATHWAY	−1.040	0.395	0.831	1.000
39	KEGG_SPHINGOLIPID_METABOLISM	−1.040	0.399	0.818	1.000
40	KEGG_DILATED_CARDIOMYOPATHY	−1.030	0.408	0.845	1.000
41	KEGG_PEROXISOME	−1.020	0.398	0.825	1.000
42	KEGG_MELANOGENESIS	−0.990	0.483	0.897	1.000
43	KEGG_GLYCOSYLPHOSPHATIDYLINOSITOL_GPI_ANCHOR_BIOSYNTHESIS	−0.980	0.459	0.913	1.000
44	KEGG_ADHERENS_JUNCTION	−0.980	0.481	0.899	1.000
45	KEGG_ETHER_LIPID_METABOLISM	−0.970	0.489	0.904	1.000
46	KEGG_INOSITOL_PHOSPHATE_METABOLISM	−0.970	0.498	0.886	1.000
47	KEGG_ARGININE_AND_PROLINE_METABOLISM	−0.940	0.526	0.948	1.000
48	KEGG_B_CELL_RECEPTOR_SIGNALING_PATHWAY	−0.930	0.552	0.963	1.000
49	KEGG_JAK_STAT_SIGNALING_PATHWAY	−0.930	0.601	0.957	1.000
50	KEGG_DRUG_METABOLISM_OTHER_ENZYMES	−0.920	0.568	0.955	1.000
51	KEGG_PYRIMIDINE_METABOLISM	−0.900	0.666	0.989	1.000
52	KEGG_FATTY_ACID_METABOLISM	−0.900	0.607	0.971	1.000
53	KEGG_SMALL_CELL_LUNG_CANCER	−0.870	0.695	1.000	1.000
54	KEGG_APOPTOSIS	−0.870	0.710	1.000	1.000
55	KEGG_NON_SMALL_CELL_LUNG_CANCER	−0.870	0.662	1.000	1.000
56	KEGG_PANCREATIC_CANCER	−0.850	0.704	1.000	1.000
57	KEGG_FC_GAMMA_R_MEDIATED_PHAGOCYTOSIS	−0.850	0.748	1.000	1.000
58	KEGG_INSULIN_SIGNALING_PATHWAY	−0.840	0.818	1.000	1.000
59	KEGG_INTESTINAL_IMMUNE_NETWORK_FOR_IGA_PRODUCTION	−0.830	0.666	1.000	1.000
60	KEGG_LYSINE_DEGRADATION	−0.830	0.722	1.000	1.000
61	KEGG_CYSTEINE_AND_METHIONINE_METABOLISM	−0.820	0.700	1.000	1.000
62	KEGG_AMINOACYL_TRNA_BIOSYNTHESIS	−0.820	0.741	1.000	1.000
63	KEGG_TGF_BETA_SIGNALING_PATHWAY	−0.810	0.778	1.000	1.000
64	KEGG_TYPE_II_DIABETES_MELLITUS	−0.810	0.755	0.996	1.000
65	KEGG_GLIOMA	−0.790	0.806	1.000	1.000
66	KEGG_PYRUVATE_METABOLISM	−0.780	0.766	1.000	1.000
67	KEGG_VALINE_LEUCINE_AND_ISOLEUCINE_DEGRADATION	−0.780	0.804	1.000	1.000
68	KEGG_PURINE_METABOLISM	−0.750	0.952	1.000	1.000
69	KEGG_VEGF_SIGNALING_PATHWAY	−0.750	0.885	1.000	1.000
70	KEGG_GLYCEROPHOSPHOLIPID_METABOLISM	−0.740	0.879	1.000	1.000
71	KEGG_TYROSINE_METABOLISM	−0.740	0.835	1.000	1.000
72	KEGG_OOCYTE_MEIOSIS	−0.720	0.964	1.000	1.000
73	KEGG_HOMOLOGOUS_RECOMBINATION	−0.720	0.847	1.000	1.000

(*continued*)

Supplementary Table S2. Continued

Negatively Deregulated DMSO

	Gene Set	NES	NOM *P*-Value	FDR q-Value	FWER *P*-Value
74	KEGG_PENTOSE_PHOSPHATE_PATHWAY	−0.710	0.814	0.992	1.000
75	KEGG_BIOSYNTHESIS_OF_UNSATURATED_FATTY_ACIDS	−0.700	0.850	0.997	1.000
76	KEGG_AMYOTROPHIC_LATERAL_SCLEROSIS_ALS	−0.670	0.936	1.000	1.000
77	KEGG_LEUKOCYTE_TRANSENDOTHELIAL_MIGRATION	−0.650	0.983	1.000	1.000
78	KEGG_NOD_LIKE_RECEPTOR_SIGNALING_PATHWAY	−0.620	0.949	1.000	1.000
79	KEGG_BUTANOATE_METABOLISM	−0.620	0.936	0.999	1.000
80	KEGG_MISMATCH_REPAIR	−0.580	0.943	1.000	1.000
81	KEGG_CELL_CYCLE	−0.570	1.000	0.994	1.000
82	KEGG_DNA_REPLICATION	−0.460	0.998	0.997	1.000

Positively Deregulated TPA

	Gene Set	NES	NOM *P*-Value	FDR q-Value	FWER *P*-Value
1	KEGG_RIBOSOME	2.250	0.000	0.000	0.000
2	KEGG_ALDOSTERONE_REGULATED_SODIUM_REABSORPTION	1.670	0.006	0.265	0.549
3	KEGG_HEMATOPOIETIC_CELL_LINEAGE	1.630	0.013	0.249	0.681
4	KEGG_NEUROACTIVE_LIGAND_RECEPTOR_INTERACTION	1.570	0.030	0.302	0.834
5	KEGG_ARACHIDONIC_ACID_METABOLISM	1.460	0.073	0.536	0.988
6	KEGG_SNARE_INTERACTIONS_IN_VESICULAR_TRANSPORT	1.370	0.087	0.788	0.999
7	KEGG_ECM_RECEPTOR_INTERACTION	1.360	0.085	0.682	0.999
8	KEGG_FOCAL_ADHESION	1.340	0.052	0.669	1.000
9	KEGG_COMPLEMENT_AND_COAGULATION_CASCADES	1.340	0.127	0.618	1.000
10	KEGG_PARKINSONS_DISEASE	1.270	0.120	0.805	1.000
11	KEGG_CARDIAC_MUSCLE_CONTRACTION	1.260	0.144	0.771	1.000
12	KEGG_OXIDATIVE_PHOSPHORYLATION	1.250	0.084	0.721	1.000
13	KEGG_ARRHYTHMOGENIC_RIGHT_VENTRICULAR_CARDIOMYOPATHY_ARVC	1.240	0.184	0.706	1.000
14	KEGG_BETA_ALANINE_METABOLISM	1.230	0.201	0.681	1.000
15	KEGG_LEUKOCYTE_TRANSENDOTHELIAL_MIGRATION	1.210	0.170	0.713	1.000
16	KEGG_REGULATION_OF_AUTOPHAGY	1.200	0.243	0.710	1.000
17	KEGG_CYTOKINE_CYTOKINE_RECEPTOR_INTERACTION	1.160	0.219	0.791	1.000
18	KEGG_PHOSPHATIDYLINOSITOL_SIGNALING_SYSTEM	1.140	0.266	0.831	1.000
19	KEGG_NATURAL_KILLER_CELL_MEDIATED_CYTOTOXICITY	1.140	0.244	0.789	1.000
20	KEGG_BUTANOATE_METABOLISM	1.110	0.324	0.831	1.000
21	KEGG_VALINE_LEUCINE_AND_ISOLEUCINE_DEGRADATION	1.100	0.335	0.822	1.000
22	KEGG_CHEMOKINE_SIGNALING_PATHWAY	1.100	0.293	0.804	1.000
23	KEGG_HYPERTROPHIC_CARDIOMYOPATHY_HCM	1.050	0.385	0.896	1.000
24	KEGG_SYSTEMIC_LUPUS_ERYTHEMATOSUS	1.050	0.378	0.890	1.000
25	KEGG_GLYCOSAMINOGLYCAN_BIOSYNTHESIS_CHONDROITIN_SULFATE	1.030	0.432	0.905	1.000
26	KEGG_INOSITOL_PHOSPHATE_METABOLISM	1.020	0.411	0.896	1.000
27	KEGG_CALCIUM_SIGNALING_PATHWAY	1.010	0.417	0.885	1.000
28	KEGG_SPHINGOLIPID_METABOLISM	1.010	0.420	0.864	1.000
29	KEGG_DORSO_VENTRAL_AXIS_FORMATION	1.000	0.448	0.868	1.000
30	KEGG_ARGININE_AND_PROLINE_METABOLISM	0.980	0.470	0.898	1.000
31	KEGG_COLORECTAL_CANCER	0.960	0.521	0.922	1.000
32	KEGG_BASAL_CELL_CARCINOMA	0.960	0.510	0.907	1.000
33	KEGG_EPITHELIAL_CELL_SIGNALING_IN_HELICOBACTER_PYLORI_INFECTION	0.940	0.535	0.922	1.000
34	KEGG_ENDOMETRIAL_CANCER	0.930	0.564	0.926	1.000
35	KEGG_TYROSINE_METABOLISM	0.910	0.554	0.962	1.000
36	KEGG_CYSTEINE_AND_METHIONINE_METABOLISM	0.890	0.605	0.983	1.000
37	KEGG_ALANINE_ASPARTATE_AND_GLUTAMATE_METABOLISM	0.890	0.620	0.967	1.000
38	KEGG_NOTCH_SIGNALING_PATHWAY	0.880	0.633	0.974	1.000
39	KEGG_GLYCINE_SERINE_AND_THREONINE_METABOLISM	0.860	0.648	0.977	1.000
40	KEGG_NEUROTROPHIN_SIGNALING_PATHWAY	0.860	0.743	0.968	1.000
41	KEGG_JAK_STAT_SIGNALING_PATHWAY	0.860	0.727	0.950	1.000
42	KEGG_ALZHEIMERS_DISEASE	0.850	0.786	0.934	1.000
43	KEGG_ERBB_SIGNALING_PATHWAY	0.840	0.746	0.933	1.000
44	KEGG_RENAL_CELL_CARCINOMA	0.830	0.786	0.939	1.000
45	KEGG_GLUTATHIONE_METABOLISM	0.790	0.778	0.991	1.000

(*continued*)

Supplementary Table S2. Continued

Positively Deregulated TPA

	Gene Set	NES	NOM *P*-Value	FDR q-Value	FWER *P*-Value
46	KEGG_GLYCEROLIPID_METABOLISM	0.780	0.807	0.989	1.000
47	KEGG_ENDOCYTOSIS	0.780	0.910	0.976	1.000
48	KEGG_FC_GAMMA_R_MEDIATED_PHAGOCYTOSIS	0.770	0.861	0.974	1.000
49	KEGG_HUNTINGTONS_DISEASE	0.750	0.968	0.974	1.000
50	KEGG_LYSOSOME	0.750	0.945	0.965	1.000
51	KEGG_PATHOGENIC_ESCHERICHIA_COLI_INFECTION	0.710	0.899	0.991	1.000
52	KEGG_PYRUVATE_METABOLISM	0.640	0.920	1.000	1.000
53	KEGG_GLYCOLYSIS_GLUCONEOGENESIS	0.580	0.985	1.000	1.000
54	KEGG_ACUTE_MYELOID_LEUKEMIA	0.550	0.993	1.000	1.000
55	KEGG_THYROID_CANCER	0.540	0.989	1.000	1.000
56	KEGG_PORPHYRIN_AND_CHLOROPHYLL_METABOLISM	0.470	0.984	0.997	1.000

Negatively Deregulated_TPA

	Gene Set	NES	NOM *P*-Value	FDR q-Value	FWER *P*-Value
1	KEGG_DNA_REPLICATION	−2.270	0.000	0.000	0.000
2	KEGG_CELL_CYCLE	−2.190	0.000	0.000	0.000
3	KEGG_HOMOLOGOUS_RECOMBINATION	−1.900	0.002	0.032	0.067
4	KEGG_OOCYTE_MEIOSIS	−1.870	0.000	0.031	0.082
5	KEGG_PYRIMIDINE_METABOLISM	−1.850	0.000	0.031	0.104
6	KEGG_MELANOMA	−1.840	0.002	0.032	0.125
7	KEGG_INTESTINAL_IMMUNE_NETWORK_FOR_IGA_PRODUCTION	−1.810	0.009	0.033	0.155
8	KEGG_MISMATCH_REPAIR	−1.680	0.013	0.105	0.460
9	KEGG_CYTOSOLIC_DNA_SENSING_PATHWAY	−1.670	0.008	0.102	0.489
10	KEGG_TYPE_I_DIABETES_MELLITUS	−1.640	0.018	0.114	0.572
11	KEGG_ALLOGRAFT_REJECTION	−1.560	0.041	0.193	0.794
12	KEGG_ADIPOCYTOKINE_SIGNALING_PATHWAY	−1.560	0.032	0.179	0.798
13	KEGG_GALACTOSE_METABOLISM	−1.550	0.029	0.179	0.823
14	KEGG_PROGESTERONE_MEDIATED_OOCYTE_MATURATION	−1.540	0.022	0.181	0.847
15	KEGG_BASE_EXCISION_REPAIR	−1.530	0.039	0.177	0.862
16	KEGG_PROSTATE_CANCER	−1.530	0.011	0.174	0.876
17	KEGG_AMINO_SUGAR_AND_NUCLEOTIDE_SUGAR_METABOLISM	−1.470	0.035	0.239	0.954
18	KEGG_P53_SIGNALING_PATHWAY	−1.460	0.038	0.245	0.961
19	KEGG_AUTOIMMUNE_THYROID_DISEASE	−1.420	0.083	0.301	0.985
20	KEGG_ANTIGEN_PROCESSING_AND_PRESENTATION	−1.390	0.065	0.336	0.994
21	KEGG_PRION_DISEASES	−1.380	0.094	0.342	1.000
22	KEGG_PURINE_METABOLISM	−1.370	0.038	0.340	1.000
23	KEGG_GAP_JUNCTION	−1.350	0.084	0.357	1.000
24	KEGG_CELL_ADHESION_MOLECULES_CAMS	−1.350	0.072	0.345	1.000
25	KEGG_MELANOGENESIS	−1.340	0.121	0.364	1.000
26	KEGG_LEISHMANIA_INFECTION	−1.330	0.084	0.362	1.000
27	KEGG_NUCLEOTIDE_EXCISION_REPAIR	−1.330	0.089	0.358	1.000
28	KEGG_LONG_TERM_POTENTIATION	−1.260	0.143	0.483	1.000
29	KEGG_LONG_TERM_DEPRESSION	−1.240	0.176	0.523	1.000
30	KEGG_VASOPRESSIN_REGULATED_WATER_REABSORPTION	−1.220	0.197	0.557	1.000
31	KEGG_LYSINE_DEGRADATION	−1.220	0.179	0.545	1.000
32	KEGG_APOPTOSIS	−1.200	0.153	0.575	1.000
33	KEGG_VIRAL_MYOCARDITIS	−1.190	0.175	0.578	1.000
34	KEGG_STEROID_BIOSYNTHESIS	−1.180	0.264	0.600	1.000
35	KEGG_GRAFT_VERSUS_HOST_DISEASE	−1.160	0.269	0.623	1.000
36	KEGG_HEDGEHOG_SIGNALING_PATHWAY	−1.160	0.275	0.617	1.000
37	KEGG_AXON_GUIDANCE	−1.150	0.220	0.633	1.000
38	KEGG_TIGHT_JUNCTION	−1.120	0.265	0.679	1.000
39	KEGG_CITRATE_CYCLE_TCA_CYCLE	−1.120	0.279	0.684	1.000
40	KEGG_GLIOMA	−1.110	0.277	0.672	1.000
41	KEGG_RNA_DEGRADATION	−1.110	0.289	0.667	1.000
42	KEGG_PANCREATIC_CANCER	−1.090	0.297	0.706	1.000
43	KEGG_REGULATION_OF_ACTIN_CYTOSKELETON	−1.080	0.257	0.712	1.000

(*continued*)

Supplementary Table S2. Continued

Negatively Deregulated_TPA

	Gene Set	NES	NOM *P*-Value	FDR q-Value	FWER *P*-Value
44	KEGG_FRUCTOSE_AND_MANNOSE_METABOLISM	−1.070	0.356	0.737	1.000
45	KEGG_DILATED_CARDIOMYOPATHY	−1.070	0.339	0.726	1.000
46	KEGG_DRUG_METABOLISM_OTHER_ENZYMES	−1.060	0.387	0.734	1.000
47	KEGG_VASCULAR_SMOOTH_MUSCLE_CONTRACTION	−1.060	0.375	0.720	1.000
48	KEGG_ABC_TRANSPORTERS	−1.050	0.380	0.713	1.000
49	KEGG_MAPK_SIGNALING_PATHWAY	−1.050	0.328	0.717	1.000
50	KEGG_TYPE_II_DIABETES_MELLITUS	−1.040	0.407	0.725	1.000
51	KEGG_NON_SMALL_CELL_LUNG_CANCER	−1.030	0.400	0.733	1.000
52	KEGG_ADHERENS_JUNCTION	−1.030	0.386	0.720	1.000
53	KEGG_PRIMARY_IMMUNODEFICIENCY	−1.030	0.416	0.708	1.000
54	KEGG_STARCH_AND_SUCROSE_METABOLISM	−1.020	0.428	0.735	1.000
55	KEGG_PATHWAYS_IN_CANCER	−1.010	0.403	0.746	1.000
56	KEGG_SPLICEOSOME	−1.000	0.440	0.752	1.000
57	KEGG_TOLL_LIKE_RECEPTOR_SIGNALING_PATHWAY	−0.990	0.463	0.753	1.000
58	KEGG_PENTOSE_PHOSPHATE_PATHWAY	−0.990	0.454	0.740	1.000
59	KEGG_VIBRIO_CHOLERAE_INFECTION	−0.980	0.482	0.769	1.000
60	KEGG_PROTEASOME	−0.960	0.510	0.807	1.000
61	KEGG_RIG_I_LIKE_RECEPTOR_SIGNALING_PATHWAY	−0.950	0.535	0.832	1.000
62	KEGG_PROPANOATE_METABOLISM	−0.940	0.541	0.822	1.000
63	KEGG_GLYCOSAMINOGLYCAN_DEGRADATION	−0.940	0.502	0.821	1.000
64	KEGG_UBIQUITIN_MEDIATED_PROTEOLYSIS	−0.940	0.599	0.820	1.000
65	KEGG_NOD_LIKE_RECEPTOR_SIGNALING_PATHWAY	−0.930	0.535	0.810	1.000
66	KEGG_TRYPTOPHAN_METABOLISM	−0.930	0.567	0.810	1.000
67	KEGG_SMALL_CELL_LUNG_CANCER	−0.930	0.591	0.802	1.000
68	KEGG_GNRH_SIGNALING_PATHWAY	−0.920	0.598	0.818	1.000
69	KEGG_WNT_SIGNALING_PATHWAY	−0.910	0.686	0.835	1.000
70	KEGG_N_GLYCAN_BIOSYNTHESIS	−0.900	0.611	0.833	1.000
71	KEGG_BLADDER_CANCER	−0.890	0.613	0.854	1.000
72	KEGG_GLYCOSYLPHOSPHATIDYLINOSITOL_GPI_ANCHOR_BIOSYNTHESIS	−0.880	0.640	0.851	1.000
73	KEGG_ONE_CARBON_POOL_BY_FOLATE	−0.850	0.621	0.914	1.000
74	KEGG_TGF_BETA_SIGNALING_PATHWAY	−0.840	0.718	0.930	1.000
75	KEGG_ETHER_LIPID_METABOLISM	−0.830	0.695	0.934	1.000
76	KEGG_INSULIN_SIGNALING_PATHWAY	−0.810	0.856	0.976	1.000
77	KEGG_T_CELL_RECEPTOR_SIGNALING_PATHWAY	−0.770	0.907	1.000	1.000
78	KEGG_B_CELL_RECEPTOR_SIGNALING_PATHWAY	−0.770	0.870	1.000	1.000
79	KEGG_RNA_POLYMERASE	−0.770	0.798	1.000	1.000
80	KEGG_CHRONIC_MYELOID_LEUKEMIA	−0.750	0.905	1.000	1.000
81	KEGG_PROTEIN_EXPORT	−0.730	0.844	1.000	1.000
82	KEGG_AMYOTROPHIC_LATERAL_SCLEROSIS_ALS	−0.710	0.910	1.000	1.000
83	KEGG_FC_EPSILON_RI_SIGNALING_PATHWAY	−0.690	0.925	1.000	1.000
84	KEGG_PEROXISOME	−0.650	0.980	1.000	1.000
85	KEGG_VEGF_SIGNALING_PATHWAY	−0.640	0.974	1.000	1.000
86	KEGG_GLYCOSAMINOGLYCAN_BIOSYNTHESIS_HEPARAN_SULFATE	−0.640	0.899	1.000	1.000
87	KEGG_PPAR_SIGNALING_PATHWAY	−0.640	0.950	1.000	1.000
88	KEGG_MTOR_SIGNALING_PATHWAY	−0.580	0.987	1.000	1.000
89	KEGG_FATTY_ACID_METABOLISM	−0.570	0.976	1.000	1.000
90	KEGG_GLYCEROPHOSPHOLIPID_METABOLISM	−0.530	0.995	1.000	1.000
91	KEGG_SELENOAMINO_ACID_METABOLISM	−0.500	0.982	1.000	1.000
92	KEGG_BASAL_TRANSCRIPTION_FACTORS	−0.500	0.998	1.000	1.000
93	KEGG_AMINOACYL_TRNA_BIOSYNTHESIS	−0.440	1.000	1.000	1.000
94	KEGG_BIOSYNTHESIS_OF_UNSATURATED_FATTY_ACIDS	−0.420	0.994	1.000	1.000

Abbreviations: FDR, false discovery rate; KEGG, Kyoto Encyclopedia of Genes and Genomes; NTC, nontargeting control; shPRKCQ, *PRKCQ* short hairpin RNA; TPA, 12-*O*-tetradecanoylphorbol-13-acetate.

Positively and negatively deregulated gene sets based on KEGG pathways of DMSO- or TPA-stimulated MyLa and HuT 78 shPRKCQ cells compared with NTC cells.

Supplementary Table S3. Clinical Data Associated with the MF Samples

Patient	Sex	Age at Diagnosis	Sample	Histopathology	% Tumoral Cells
MF1	Female	56	MF1.1	Plaque	5
			MF1.2	Plaque	15
			MF1.3	Tumor	90
MF2	Male	58	MF2.1	Tumor	90
			MF2.2	Plaque	15
			MF2.3	Tumor	80
			MF2.4	Plaque	90
			MF2.5	Tumor	90
MF3	Female	53	MF3.1	Tumor	90
			MF3.2	Plaque	5
			MF3.3	Plaque	10
			MF3.4	Plaque	8
			MF3.5	Tumor	80
MF4	Male	50	MF4.1	Plaque	5
			MF4.2	Plaque	10
MF5	Male	65	MF5.1	Plaque	15
			MF5.2	Tumor	80
MF6	Male	36	MF6.1	Plaque	20
			MF6.2	Plaque	10
			MF6.3	Plaque	15
			MF6.4	Plaque	40
			MF6.5	Plaque	10
MF7	Male	64	MF7	Tumor	30
MF8	Male	71	MF8.1	Plaque	5
			MF8.2	Tumor	90
			MF8.3	Tumor	90
MF9	Female	45	MF9.1	Plaque	20
			MF9.2	Tumor	80
			MF9.3	Tumor	90
			MF9.4	Plaque	20
			MF9.5	Tumor	90
			MF9.6	Plaque	15
MF10	Female	58	MF10.1	Plaque	N/D
			MF10.2	Plaque	N/D
MF11	Female	41	MF11	Plaque	N/D
MF12	Female	70	MF12.1	Plaque	5
			MF12.2	Plaque	10
			MF12.3	Plaque	10
			MF12.4	Plaque	7
			MF12.5	Plaque	10
			MF12.6	Plaque	40
			MF12.7	Plaque	30
			MF12.8	Plaque	15
			MF12.9	Plaque	10
			MF12.10	Tumor	90
MF13	Male	16	MF13.1	Plaque	15
			MF13.2	Plaque	10
			MF13.3	Plaque	5
MF14	Male	32	MF14.1	Plaque	5
			MF14.2	Plaque	5
MF15	Male	37	MF15.1	Plaque	15
			MF15.2	Plaque	10
MF16	Male	54	MF16.1	Plaque	15
			MF16.2	Plaque	20
			MF16.3	Plaque	20
			MF16.4	Tumor	80
MF17	Male	56	MF17	Plaque	5

(*continued*)

Supplementary Table S3. Continued

Patient	Sex	Age at Diagnosis	Sample	Histopathology	% Tumoral Cells
MF18	Female	76	MF18.1	Plaque	10
			MF18.2	Plaque	20
			MF18.3	Tumor	80
MF19	Female	56	MF19	Plaque	10
MF20	Male	47	MF20.1	Plaque	5
			MF20.2	Plaque	10
			MF20.3	Plaque	10
MF21	Male	32	MF21	Plaque	20
MF22	Female	59	MF22.1	Plaque	20
			MF22.2	Plaque	15
			MF22.3	Plaque	20
			MF22.4	Plaque	15
MF23	Male	14	MF23.1	Plaque	5
			MF23.2	Plaque	10
			MF23.3	Plaque	10
MF24	Male	32	MF24	Plaque	10
MF25	Female	77	MF25.1	Plaque	15
			MF25.2	Tumor	80
MF26	Male	61	MF26.1	Plaque	15
			MF26.2	Plaque	20
			MF26.3	Tumor	95
			MF26.4	Plaque	30
MF27	Female	31	MF27.1	Plaque	15
			MF27.2	Plaque	15
INF1	Male	73	N/A	Inflammatory dermatoses	N/A
INF2	Male	49	N/A	Inflammatory dermatoses	N/A
INF3	Male	74	N/A	Inflammatory dermatoses	N/A
INF4	Male	38	N/A	Inflammatory dermatoses	N/A
INF5	Female	72	N/A	Inflammatory dermatoses	N/A
INF6	Male	36	N/A	Inflammatory dermatoses	N/A

Abbreviations: MF, mycosis fungoides; N/A: not applied; N/D: not determined.